Quarterly Progress Report

Radar Studies of the Moon

15 February 1966

Issued 8 April 1966

Lincoln Laboratory

MASSACHUSETTS INSTITUTE OF TECHNOLOGY

Lexington, Massachusetts

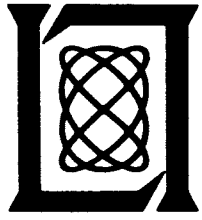

FOREWORD

This is the first quarterly progress report required under Contract NSR 22-009-106 between the National Aeronautics and Space Administration and Lincoln Laboratory, M.I.T. This contract calls for radar and radiometric studies of the moon, with a view to determining the nature of the lunar surface. Extensive radar studies of the moon have been made at Lincoln Laboratory since 1958, and elsewhere prior to that date. Thus the planned program of work is based upon these earlier studies and seeks to extend them, either with new types of measurements or by repeating earlier ones with greater resolution.

To help the reader to understand the planned program and to appreciate the number of remarkable results concerning the lunar surface which have already been obtained by radar, we shall summarize in Sec. I of this report most of the radar studies of the moon to date. Future reports of this series will be written upon the assumption that the reader is familiar with the material in this report and frequent reference will be made to it.

Section II covers certain highlights of the research conducted during the period from 1 October 1965 through 31 January 1966,* mentioning particularly the experiments that most recently contributed to the picture presented in Sec. I.

Section III reviews in some detail the up-to-date planning of the experimental program as influenced by the most recent results, which have had a profound bearing on our ideas concerning the nature of the lunar surface, and the interpretation of earlier results.

* Subsequent reports will cover three- rather than four-month intervals.

CONTENTS

I. RADAR STUDIES OF THE MOON

This section reviews in some detail studies of the moon conducted during the past decade, including most of the important observational and related theoretical work. Based upon this work, it now appears that the lunar surface is covered almost everywhere by a layer of light material. The dielectric constant of this material appears to be about 1.8, implying a porosity in the range from 70 to 90 percent. The depth of this material is unknown, but could be inferred from earth-based radar measurements. The present measurements merely permit us to place a lower limit on the depth of the order of 20 cm.

The nature of the supporting layer is as yet ill determined. The existing measurements do not permit us to decide between a model of the surface in which the density increases gradually with depth, or abruptly as a solid surface is encountered. If the latter "two layer" model is accepted, it can be shown that the dielectric constant of the supporting layer is about 5, implying that if the material here is solid it must consist largely of silicates or other materials of low dielectric constant.

The distribution of surface slopes for the lunar surface has been determined for a number of scale intervals (set by the exploring wavelength). The distribution obtained at 1-meter (m) wavelength is roughly the sum of the distributions for the top and supporting layers (if the two-layer hypothesis is considered). At this wavelength (1 m), the mean surface slope is about 10°. This value applies to points spaced of the order of 5 to 10 wavelengths (5 to 10 m) apart, and thus would be a suitable value to use in the design of a lunar landing vehicle. Approximately 20 percent of the area of the moon's surface appears to be covered by structure which has horizontal and vertical scales comparable with one meter. This structure may represent either features lying upon the supporting surface or density irregularities lying within the upper layer. As the exploring wavelength is shortened, the surface appears more irregular, though still relatively smooth at a wavelength of 3.6 cm (mean slope = 15°). At 8-mm wavelength, the surface appears almost completely rough – as it does optically. It must be expected that these measurements apply almost entirely to the upper layer, owing to the inability of short-wavelength rays to penetrate as readily as longer waves.

Whereas the above represents a brief description of the average properties of the lunar surface inferred from radar measurements, additional information concerning different visual features is also available. At a wavelength of 1 m, the highlands appear 50 percent more reflective than the mare. The explanation of this may be that the light material has a greater depth in the mare than on the highlands, or there may be significant differences in the types of rocks and/or relative roughness in the two areas. Unfortunately, it is not yet possible to decide between these competing explanations. Probably a combination of at least two is involved.

Radar "mapping" carried out at the Arecibo Ionospheric Observatory has shown that all the rayed craters and bright "new looking" craters are anomalous reflectors in the sense that they are considerably better scatterers than a comparable area in their environs. Since this enhancement is found both for the expected polarization (i.e., that reflected by a plane mirror)

and for the depolarized component, we are forced to conclude that in these craters the material is considerably denser than elsewhere. It is probable that only in these craters is solid rock exposed to the surface. The most outstanding example of this behavior is the crater Tycho, where the enhanced reflectivity is ten times that of the surrounding terrain. Separate measurements have confirmed the absence of a layer of light material overlying Tycho (at least in excess of one or two centimeters deep). In part, the anomalously strong reflections from these craters may also be explained by the increased roughness caused by the primary impact, which has fractured and torn the surface and deposited boulders over a large region beyond the crater walls. Conversely, the large difference between the intensity of the signals reflected from Tycho and the surrounding mare material reinforces the view (obtained from alternate evidence) that most of the lunar surface is smooth, gently undulating, and has a very porous uppermost surface.

A. INTRODUCTION

The smallest objects on the lunar surface that are resolvable by means of large ground-based optical telescopes have dimensions of the order of $\frac{1}{2}$ km. At the other extreme, photometric studies (Hapke and Van Horn, 1963)* and polarization measurements (Dollfus, 1962) yield information about the microstructure, which may at most be measured in millimeters. The success of manned exploration of the lunar surface may depend to a great extent upon the nature of the surface in the range of sizes between these two extremes. If the surface were densely covered with new craters below the optical limit of resolution, or for that matter boulders of a size comparable with a landing vehicle, severe difficulties would be encountered. Until close-proximity photographs were obtained (Heacock, et al., 1965), one could be guided only by radar results. These suggested that the surface is not necessarily very hostile – a result that has partly been confirmed by the Ranger pictures.

A historical review of the early radar observations of the moon has been given by Evans (1962a), and here we shall present only what seems the best available experimental evidence concerning the moon's scattering behavior. For the most part, this has been obtained by measuring the distribution of the echo power as a function of range delay, using short pulse transmissions. Additional measurements in which both the delay and Doppler resolution of the radar are exploited have shown that, though the larger part of the moon's surface is rather featureless to radar observation, the newer (rayed) craters are extraordinarily bright with respect to their surroundings. When further experiments are conducted in which delay and Doppler resolution are employed together with the ability to control the polarization of the transmitted and received signals, we find evidence for a layer of light tenuous material overlying most parts of the surface.

The experimental observations described have stimulated a large number of theoretical workers to attempt to deduce from the scattering properties of the moon a statistical description of its surface structure. We shall outline two of the approaches that have been taken to relate the surface properties to the scattering behavior. These two approaches lead essentially to the same result: the probability distribution of surface slopes is related to the distribution of echo power with delay observed for very short pulse transmissions.

* References for this report are arranged alphabetically on pages 68-71.

The experimental work reviewed here is presented roughly in the order of the complexity of the measurements. Thus we consider first (Sec. I-B) the measurement of total echo power and the factors governing the radar cross section which can be determined from such measurements. Later we discuss the fading characteristics of moon echoes (Sec. I-D) and the distribution of the echoes in delay as observed with a short pulse radar (Sec. I-E). Both these observations lead to a determination of the brightness distribution of the echoes over the lunar disk, or to a related quantity, the angular power spectrum of the echoes. This last function yields, via appropriate theory (Sec. I-F), a statistical distribution of the surface slopes on the moon (Sec. I-G). In Sec. I-H, we review the methods and results of experiments to map the radar reflectivity over the lunar disk, and thereby determine the location and identity of unusually strong or weak reflectors. Experiments in which the polarizations of the transmitted and received signals are controlled in order to explore the influence of the angle between the plane containing the electric field and the mean surface are described in Sec. I-J. These experiments yield a value for the dielectric constant of the surface material (Sec. I-K) which in turn enables one to place limits on the relative density (packing factor) of that material (Sec. I-L). Section I-M provides a summary of Sec. I.

B. TOTAL ECHO POWER

1. Radar Equation for Distributed Target

The radar equation as normally stated is applicable to "point targets," i.e., objects which when viewed from the radar subtend an angular diameter much smaller than that of the antenna beam. In this case, the received echo power P_r may be stated as

$$P_r = \frac{P_t G A \sigma}{(4\pi R^2)^2} \text{ watts} \tag{1}$$

where P_t is the transmitted power (watts), G is the antenna gain, A is the antenna aperture (m^2), σ is the cross section of the target (m^2), and R is the target's range (m). Of all the celestial objects studied by means of radar, the moon and the sun are the only ones in which the target angular diameter is likely to be as large or larger than the antenna beam. The cross section σ observed during observations of the moon, therefore, depends upon the distribution of the incident power over the surface. In practice, the moon reflects preferentially from regions near the center of the disk and little loss in total reflected power will be observed until the antenna beamwidth (between half-power points) is made smaller than the angular extent of the moon ($\frac{1}{2}^\circ$). Thus for parabolic antenna systems, this effect will not be important until the antenna diameter becomes larger than 100λ, where λ is the radio wavelength.

All the nearby objects in the solar system, however, can be resolved in range and/or in frequency. It is readily possible to transmit pulses which are of insufficient length to illuminate the whole of a planet's visible hemisphere. A pulse of 11.6 msec is required to fully illuminate the surface of the moon, and if shorter pulses are employed, the effective or instantaneous cross section σ will never reach its maximum possible value (the CW cross section). Figure 1 shows how the peak instantaneous cross section falls as a function of pulse length for observations of the moon at a wavelength of 68 cm. Because the largest part of the power is reflected from the

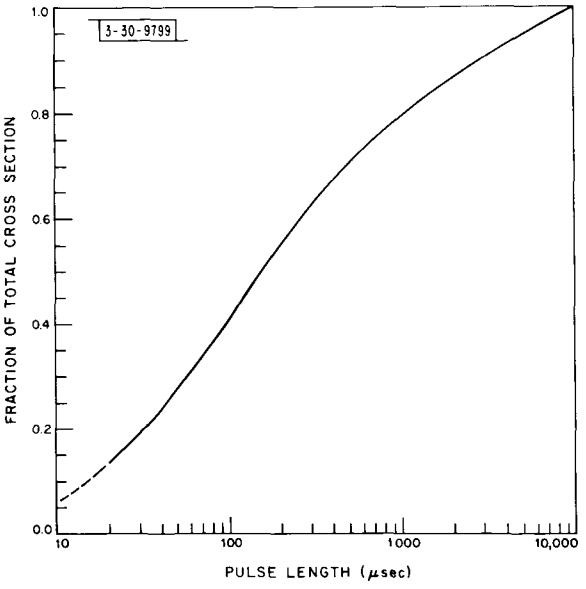

Fig. 1. Peak cross section of the moon expressed as percentage of total cross section σ plotted as a function of pulse length. Radar depth of the moon is 11.6 msec and if pulses shorter than this are employed, echo power will fall owing to reduction in instantaneous area illuminated by pulse.

nearest regions of the lunar surface, a significant reduction in cross section is not observed until a pulse of 1-msec duration is used. Figure 1 is applicable only for wavelengths of about 50 cm or longer, because the scattering properties of the surface change markedly toward shorter wavelengths. Equally, where a CW radar is employed, the rotation of the planet may cause the reflected signals to be appreciably Doppler broadened. If the receiver employs a narrow-band filter which does not accept all the frequency components of the reflected signal, again the observed cross section will be lower than the full value.

For the remainder of this section, we shall use the term σ to denote the total cross section of the moon. This could be measured with a radar employing an antenna beam of $\frac{1}{2}^\circ$ or more by determining the peak echo power observed when pulses of 11.6 msec or longer are transmitted. In practice, echoes from the moon are found to fade (Sec. I-C) as a consequence of constructive and destructive interference between signals arriving from different parts of the lunar surface. Thus, an average value for the peak echo power (or mean square of the echo amplitude) must be obtained from many pulses to determine σ reliably. Alternatively, with a CW radar, many independent determinations of the echo power are required. In some of the earliest radar observations of the moon (e.g., DeWitt and Stodola, 1949), this was not recognized and only the maximum value of the echo intensity was reported.

When the antenna beamwidth is comparable with the diameter of the moon, it is possible to compute σ if the distribution of incident power over the surface is known (defined by the antenna pattern) and the brightness distribution observed for the lunar disk for uniform illumination is also known. Thus, if the axis of the antenna beam is directed at the center of the moon and the antenna pattern is circularly symmetrical about this axis, the echo power is given by

$$P_r = \frac{P_t G^2 \lambda^2 \sigma}{64\pi^3 R^4} \int_\Theta A^2(\Theta) B(\Theta) 2\pi \sin\Theta \, d\Theta \qquad (2)$$

in which λ is the radio wavelength. Here Θ is the angle subtended at the radar between the beam axis and an annulus of width $d\Theta$ on the lunar surface, $A(\Theta)$ is the normalized antenna

$$Q = \frac{1 - \sqrt{\frac{\mu_o}{\mu}\left(\frac{\epsilon}{\epsilon_o} + i\,\frac{s}{\omega\epsilon_o}\right)}}{1 + \sqrt{\frac{\mu_o}{\mu}\left(\frac{\epsilon}{\epsilon_o} + i\,\frac{s}{\omega\epsilon_o}\right)}} \tag{6}$$

ϵ is the permittivity, μ is the permeability, s is the conductivity (the subscript o denotes free space values) and ω is the angular radio-wave frequency. It can be seen that $\rho_o (= |Q|^2)$ will depend on the wavelength, unless s is zero or infinite. For a perfect dielectric, where $\mu \to \mu_o$ and $s \to 0$, Eq. (6) simplifies to

$$Q = \frac{1 - \sqrt{k}}{1 + \sqrt{k}} \tag{7}$$

where $k = \epsilon/\epsilon_o$ is the relative dielectric constant. Values of k for some typical rock mineral samples are given in Table I. These have been taken from many values listed in a report by Brunschwig, et al. (1960). The selection in Table I is somewhat arbitrary, but does indicate the wide scatter of values encountered. The basaltic specimens examined by Brunschwig showed the greatest range of values (from 5.5 to 26.7) and an average value for the seven samples listed is 14. For the minerals listed as forms of andesite (5 samples), the mean was 8.8, while the

TABLE I
DIELECTRIC CONSTANTS FOR VARIOUS MATERIALS

Mineral	Type	Source	Dielectric Constant k
Andesite	Vesicular Basalt	Chaffee County, Colorado	6.51
Olivine Basalt Cellular		Washington	5.50
Basalt	Olivine Basalt	Jefferson County, Colorado	8.89
Olivine Basalt	Basalt	Lintz, Rhenish Prussia	17.4
Diabase		Mt. Tom, Massachusetts	10.8
Rhyolitic Pumice	Pumice	Millard County, Utah	2.29
Rhyolite		Castle Rock, Colorado	4.00
Basaltic Scoria	Scoria	Near Klamath Falls, Oregon	6.08
Trachytic Tuff		Near Cripple Creek, Colorado	5.32
Quartz Sandstone	Sandstone	Columbia County, Pennsylvania	4.84

pattern (power vs angle, $A(\Theta) = 1$ for $\Theta = 0°$) and $B(\Theta)$ is the angular distribution of radar cross section that would be observed with a broad-beam antenna. $B(\Theta)$ is normalized so that the integral in Eq. (2) tends to unity for broad-beam antennas. The term $A(\Theta)$ appears as a square term, since the antenna weights the transmission and reception equally.

When the antenna beam is broad but the pulse length τ is shorter than the radar depth of the moon, the echo power is given in

$$P_r = \frac{P_t G A \sigma}{(4\pi R^2)^2} \int_0^{\tau} \overline{P}(t)\, dt \tag{3}$$

where $\overline{P}(t)$ is the average distribution of the echo power with delay t (relative to the leading edge of the moon) measured with a short, square pulse τ' as $\tau' \to 0$ (it is sufficient for $\tau' \ll \tau$). The integral in Eq. (3) becomes unity for $\tau \geqslant 11.6$ msec. The general case in which the antenna beam is smaller than the diameter of the moon and short pulses are employed has been treated (Evans, 1962b) by graphically integrating areas inside contours of equal incident energy and equal range. By repeating the observations for different positions of the antenna beam with respect to the moon's center, it was possible to recover $\overline{P}(t)$ and thence σ.

2. Effect of Range Variations on Total Power

The mean range of the moon is 3.844×10^8 meters (causing an echo delay of 2.56 sec) but due to the ellipticity of the moon's orbit, the actual range may vary over ±8 percent of the mean range. As a result, the echo power will vary over a lunation by ±30 percent (about ±1 db). The accuracy achieved in most radar experiments is insufficient for this to be detected, and Fricker, et al. (1958) appear to be the only workers who have observed this variation of echo power during the month. Even they were unable to observe the small variation (about 0.2 db) introduced by the rotation of the earth. These range changes are easily detected by measuring the echo delay time. Very accurate measurements have been made by Yaplee, et al. (1958) and these are reviewed in Sec. I-C.

The difference between the echo power expected on a given day and the mean echo power is given by

$$\Delta P = 40(\log_{10} \pi - 1.756) \text{ db} \tag{4}$$

where π is the daily value of the equatorial horizontal parallax tabulated in The American Ephemeris and Nautical Almanac for the appropriate year in minutes of arc.

3. Theoretical Values of Cross Section

If the moon were a perfect sphere having a power reflection coefficient at normal incidence of ρ_o, the cross section would be (Senior and Siegel, 1959)

$$\sigma = \rho_o \pi a^2 \tag{5}$$

provided, of course, that the radius $a \gg \lambda$, where λ is the exploring wavelength. The reflection coefficient ρ_o is related to the electrical constants of the surface $\rho_o = |Q|^2$ where

rhyolitic samples were lower (4.1). Silicate materials, e.g., fused quartz, are frequently suggested as making up the bulk of the lunar surface material and these silicates have dielectric constants which range from 5 to 7.* Dry terrestrial sand has a dielectric constant of about half this amount.

The electrical conductivity s of the lunar surface material is not known. If s is not negligible, we should expect the reflection coefficient ρ_o to decrease with increasing frequency ω (Eq. 6). Such a decrease could be difficult to observe in the data, for as we shall show, several other effects probably influence the values of cross section as a function of wavelength by a larger amount. For terrestrial rock powders, the conductivity is largely determined by the dryness of the material. That is, most of the current flows over the surface of the grains via occluded water molecules. Since the moon is known to lack any measurable atmosphere, it seems reasonable to assume that the surface is exceedingly dry and that as a result s is small. Thus, in the absence of any better evidence, we shall employ Eq. (7) in place of Eq. (6) throughout this report. We recognize, however, that this approximation might not be valid, if, for example, the lunar soil contains a large proportion of metallic ores introduced perhaps by meteoritic bombardment or alternatively if grains of the lunar soil are coated with reduced metal (as suggested by Gold) as a result of proton bombardment. If the surface of the moon were solid rock having a dielectric constant k = 5 (the lowest value likely), the reflection coefficient would be 14 percent.

If the perfect sphere discussed above is replaced by one in which the true surface departs in an irregular fashion from the mean, then the cross section is likely to change and account can be taken of this by writing

$$\sigma = g\rho_o \pi a^2 \quad . \tag{8}$$

Here g is a directivity factor that expresses the ability of the sphere to scatter back favorably toward the source. For a smooth metal sphere ($\rho_o = 1$), the echo power is re-radiated isotropically and the value of g is 1.0 (Norton and Omberg, 1947). As we have seen, the factor g is also unity for a smooth dielectric sphere, but the scattering is not isotropic and depends upon the dielectric constant k (Rea, et al., 1964).

The value for g as defined by Eq. (8) for an arbitrarily rough surface is not known and only the sphere with a smooth, undulating surface has been examined in detail (Hagfors, 1964). In this case, $g = 1 + \alpha^2$, where α is the rms surface slope. The shallow undulations cause rearrangement in the pattern of Fresnel zones at the center of the disk so that parts of each zone are distributed randomly over the entire disk. Provided that the antenna beam is broad enough to illuminate the whole surface, a small increase in mean cross section will be observed when this hypothetical, ideally-smooth sphere is replaced by one with an undulating surface.

An alternate and widely adopted approach to obtaining the scattering cross section is to consider the scattering properties of the target as specified by a function $\sigma_o(i\varphi\Theta)$ which defines

* An alternative argument due to Gold (1964) is to suppose that fractionation processes have not occurred in lunar rocks to the extent that they have on earth. The surface rocks would then be expected to differ little from meteoritic material and to have a high dielectric constant (k ~ 20).

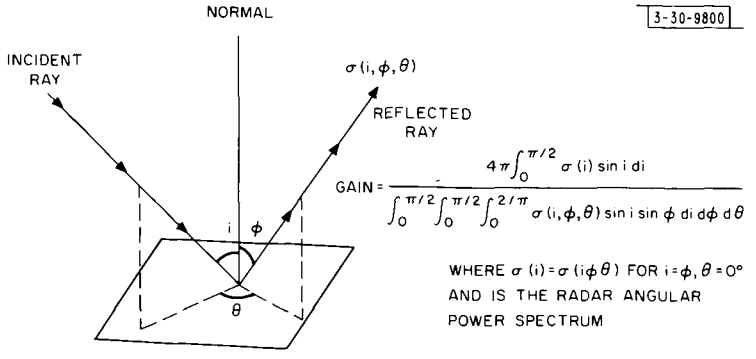

Fig. 2. Geometry required for studying complete scattering characteristics of an irregular surface in order to obtain a value for gain of whole moon over an isotropic scatterer.

the reflected intensity per unit surface area per steradian. This function is obtained by exploring the power reflected from an elemental area of surface illuminated at an angle of incidence i, and observed at an angle of reflection φ; the planes containing these two rays and the surface normal are at an angle Θ as shown in Fig. 2. Provided there is no coherence between returns from different surface elements, the gain G_m of the moon in the direction of backscattering is given by

$$G_m = \frac{4\pi \int_0^{\pi/2} \sigma_o(i) \sin i \, di}{\int_0^{\pi/2} \int_0^{\pi/2} \int_0^{2\pi} \sigma_o(i\varphi\Theta) \sin i \sin\varphi \, d\Theta \, d\varphi \, di} \tag{9}$$

where $\sigma(i)$ is the limited case in which $i = \varphi$ and $\Theta = 0$. From earth-based observations alone, only $\sigma_o(i)$ can be determined; hence, G_m as defined by Eq. (9) cannot be obtained. If, however, G_m were known either from theory or observation, the cross section for the whole sphere could be written as

$$\sigma = G_m \bar{\rho} \cdot \pi a^2 \quad . \tag{10}$$

Here $\bar{\rho}$ is the albedo averaged over the hemisphere, and this usually differs from the reflection coefficient at normal incidence ρ_o. This distinction has not always been recognized and the literature contains several instances where ρ_o has been equated with $\bar{\rho}$ without proper explanation. If this is done, the directivity factor g is automatically made the same as G_m. Rea, et al. (1964) have pointed out that these approximations are certainly not valid for the smooth dielectric sphere.

Some comments are appropriate here on values for the gain G_m which have appeared in the literature. Kerr and Shain (1951) assumed that the moon was a uniformly bright reflector and deduced a value for $G_m = 5.7$ from the variation of the moon's optical brightness with phase. The moon is nine times as bright at full moon as at quarter phase, because all parts of the surface have the property of scattering preferentially back in the direction of the source. Such behavior is believed to be a consequence of the microrelief on the surface which contains many interconnected cavities (Hapke and Van Horn, 1963). It is therefore a shadowing effect which could

occur at radio wavelengths, if the surface elements were largely smooth but arranged at a wide variety of slopes to one another. Thus, near the limb only those areas which were normal to the line of sight would be seen and these would screen from view regions which would not scatte: favorably to the observer. The uniformly bright behavior of the moon observed optically is discussed by Schoenberg (1929), Hapke (1963), and others. A very approximate expression for this type of scattering is contained in the Lommel-Seeliger law

$$\sigma_{LS} \propto \frac{\cos i}{\cos i + \cos \varphi} \quad . \tag{11}$$

Where a surface is covered with structure (e.g., boulders) comparable in both horizontal and vertical dimensions to the radar wavelength, it will scatter according to the Lambert law

$$\sigma_L \propto \cos \varphi \cos i \quad . \tag{12}$$

The disk of a spherical object obeying Lambert's law will appear slightly limb dark and will exhibit a gain factor $G_m = 8/3$ (Grieg, et al., 1948). If the observed scattering law can be expressed as

$$\sigma_o(i \varphi \Theta) \propto \cos^m i \cos^n \varphi \tag{13}$$

then

$$G_m = \frac{2(m + 1)(n + 1)}{(m + n + 1)} \tag{14}$$

provided again that there is no coherence between the signals returned from any of the surface elements (Pettengill, 1961). This restriction is important, since for an ideally smooth moon, we would have in Eq. (14) m and $n \to \infty$ causing $G_m \to \infty$. Evidently, Eq. (14) holds only for smal values of m and n.

4. Observed Values of Cross Section

Many observers have reported values of σ and some of these values are presented in Table II and plotted in Fig. 3. The values have been presented as fractions of the physical cross section of the moon ($\pi a^2 = 9.49 \times 10^{12}\ m^2$), and span a range of over ten octaves (from 8.6 mm to 22 meters). The increase in cross section with increasing wavelength suggested by Fig. 3 depends largely on the three long-wave measurements reported by Davis and Rohlfs (1964). These measurements may have been subject to systematic errors introduced by ionospheric effects. If these three points are ignored, the remainder show no clear wavelength dependence. In part this is caused by the large error bars associated with each measurement, which may conceal a marked dependence. The errors given in Table II are reported values where these have been given, or ±3 db where no uncertainty was published. Absolute power measurements appear to be more difficult in radar astronomy observations than in radio astronomy observations for several reasons. In the first place, the uncertainty in the antenna performance (typically ±1 db) enters twice. Next, there is the uncertainty associated with measuring the transmitted power P_t, and finally, errors arise in the measurement of the echo power P_r owing in part to the fading of the signals. Unless extraordinary care is taken, the uncertainty in

TABLE II

VALUES FOR RADAR CROSS SECTION OF THE MOON AS A FUNCTION OF WAVELENGTH REPORTED BY VARIOUS WORKERS

Author	Year	Wavelength (cm)	$\sigma/\pi a^2$	Estimated Error (db)
Lynn, et al.	1963	0.86	0.07	±1
Kobrin	1963†	3.0	0.07	±1
Morrow, et al.	1963†	3.6	0.07	±1.5
Evans and Pettengill	1963a	3.6	0.04	±3
Kobrin	1963†	10.0	0.07	±1
Hughes	1963†	10.0	0.05	±3
Victor, et al.	1961	12.5	0.022	±3
Aarons	1959‡	33.5	0.09	±3
Blevis and Chapman	1960	61.0	0.05	±3
Fricker, et al.	1960	73.0	0.074	±1
Leadabrand	1959‡	75.0	0.10	±3
Trexler	1958	100.0	0.07	±4
Aarons	1959‡	149.0	0.07	±3
Trexler	1958	150.0	0.08	±4
Webb	1959‡	199.0	0.05	±3
Evans	1957	250.0	0.10	±3
Evans, et al.	1959	300.0	0.10	±3
Evans and Ingalls	1962	784.0	0.06	±5
Davis and Rohlfs	1964	1130.0	0.17	+3 −2
Davis and Rohlfs	1964	1560.0	0.12	+3 −2
Davis and Rohlfs	1964	1920.0	0.16	+3 −2

† Revised value (privately communicated).

‡ Reported by Senior and Siegel, 1959 and 1960.

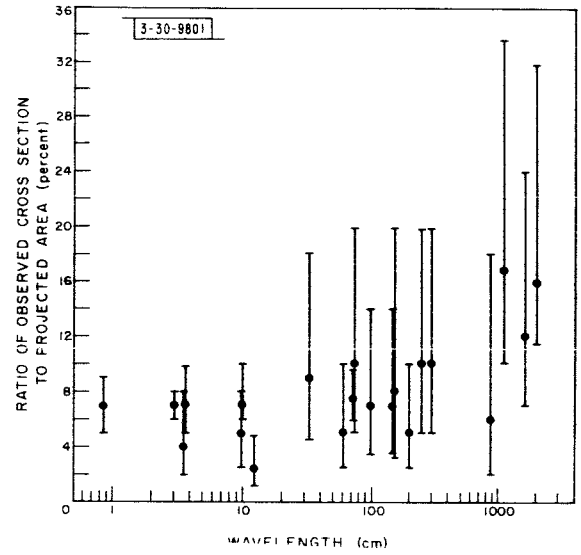

Fig. 3. Variation of total cross section σ as a function of radar wavelength λ. These values are expressed as a fraction of the moon's projected disk πa^2 and were obtained from papers listed in Table II.

absolute intensity is usually of the order of ±3 db. That Fricker, et al. (1958) are the only observers who have reported observations of the monthly variation of P_r (which is 2 db) is indicative of the difficulties encountered. Even in the case of Fricker's results, it was not possible to determine the absolute value of P_r to better than ±1 db. Because the moon is an extended target whose characteristics change with wavelength, it does not serve radar astronomers as a reference in the manner that certain radio sources (e.g., Cygnus A) are used by radio astronomers. Radar astronomy will benefit from the orbiting spherical reflector Lincoln Calibration Sphere (LCS) which provides a 1-m^2 standard test target at an altitude of 1500 nautical miles (n.mi). By calibrating each radar by means of this sphere, any wavelength dependence in the lunar cross section should be obtainable with greater confidence.

The mean of the values listed in Table II is close to 0.07 and using this mean value, the term $\sigma/(4\pi R^2)^2$ has a value of about 1.95×10^{-25} m^{-2}. This term represents the "path loss" encountered by a signal transmitted by an antenna of unit gain, reflected by the moon and received by an antenna of unit aperture. Expressed in this fashion, the path loss is independent of wavelength and may be taken as 247.2 db/m^2.

The observed values for the cross section σ cannot immediately be used to derive the reflection coefficient ρ and thence the dielectric constant k [via Eq. (7)] because of the uncertainty in the value that should be taken for the gain g in Eq. (8). Thus we return to this point later (in Sec. I-K), after some results bearing on the value of g have been presented.

C. THE MOON'S MOTIONS

1. Range Measurements

The radar distance to the moon can readily be determined with high precision, but because the moon's distance has been determined by optical methods over a long period of time, it is difficult to make a significant improvement by using radar. Only one group of workers (Yaplee, et al., 1958, 1959) has been actively engaged in these measurements over an extended period. This group at the Naval Research Laboratory employs a 50-foot parabola, together with a 10-cm

radar (2860 MHz) having a peak power of 2 Mw and a pulse length of 2 μsec. The accuracy of measurement is limited by the fading of the echo, making it difficult to recognize with absolute certainty the reflection corresponding to the nearest point on the surface of the moon.

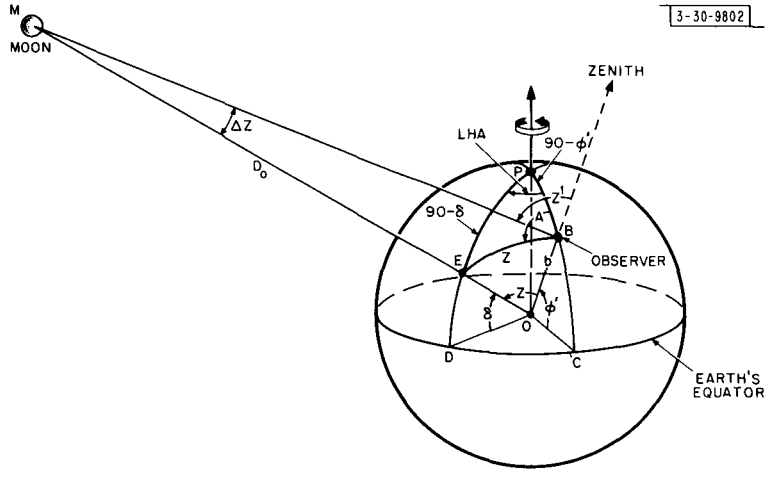

Fig. 4. Geometry involved in radar range measurements of distance of the moon from point on earth's surface.

Figure 4 shows the relevant geometry for these measurements. The quantities involved principally are the earth's equatorial radius r and the equatorial horizontal parallax π. The measured radar distance BM in Fig. 4 is given by

$$BM = -a + (b^2 + D_o^2 - 2bD_o \cos z) \tag{15}$$

in which

$$\cos z = \sin \varphi' \sin \delta + \cos \varphi' \cos \delta \cos HA$$

a = lunar radius to the subradar point

b = observer's radius vector

D_o = predicted center-to-center distance = $r/\sin \pi$

r = earth's equatorial radius

π = moon's equatorial horizontal parallax

φ' = geocentric latitude of the station

δ = moon's declination.

The value of b can be obtained from the elliptic formula

$$b = \frac{r(1-f)}{\sqrt{1-(2f-f^2)\cos^2 \varphi}} + H \tag{16}$$

in which the oblateness constant f may be taken as 1/298.3 and H is the height of the antenna above sea level.

Yaplee, et al. (1958) found that the value for the equatorial radius adopted by the U.S. Army map service was inconsistent with their observations, but that given by The American Ephemeris

and Nautical Almanac (r = 6,378,388 meters) was in better agreement. Later, Yaplee, et al. (1959) showed that residual errors (observed – computed range) of about 3 km were encountered and that these were not the same from day to day.

After continuing their observations for some considerable time, Yaplee, et al. (1964) adopted the following constants: the velocity of light $c = 2.997928 \times 10^8$ m/sec, a = 1738 ● 1 km, r = 6,378,170 m. They observed that the radar distance depended directly upon the height of the topography of the subradar point. Accordingly, they adjusted the value for the effective lunar radius a according to the height of the subradar point as given by an equivalent optical map obtained by the Naval Research Laboratory from the Army map service (Fig. 5). The best value of D_o was then obtained by a least-mean-square solution to the range residuals. For the mean center-to-center distance $\overline{D}_o$, Yaplee, et al. (1964) obtained $\overline{D}_o = 384{,}400.2 \pm 1.1$ km. The best corresponding optical determination (O'Keefe and Anderson, 1952, 1958) is $\overline{D}_o = 384{,}400 \pm 4.7$ km.

It is obvious that by continuing this work over many lunar cycles, the elements of the moon's orbit may be refined. In principle, the figure of the earth could be redetermined from observations conducted from many points on the earth. What would be of more interest to astronomers is the determination of the moon's figure and this cannot readily be accomplished by present-day radar methods. It seems that this must await the introduction of sophisticated laser radar systems or lunar orbiting satellites.

2. Doppler Shifts

Because the moon moves in an elliptical orbit it will, in general, have a component of velocity toward the center of the earth. This has a maximum value

$$v_1 = \frac{2\pi \times 30{,}600\ \text{km}}{28\ \text{days}} = \pm 80\ \text{m/sec} \quad .$$

In addition, an observer on the earth will have a velocity component v_2 due to the rotation of the earth given by

$$v_2 = \pm \frac{2\pi\ \text{earth's radius} \times \cos\varphi' \times \cos\delta \times \sin \text{HA}}{\text{earth's rotation relative to the moon}}$$

where φ' is the observer's latitude, δ the moon's declination and HA the local hour angle. The maximum value of v_2 (occurring on the equator at moonrise or moonset) is about ±500 m/sec. The Doppler shift d_2 due to the component of velocity v_2 can readily be calculated for any station as a function of hour angle HA. It will be found that the change in the moon's declination over the month introduces changes in d_2 that are less than about 10 percent. The component d_2 must be added (with regard to sign) to the component d_1 introduced by v_1 which can be computed approximately from

$$d_1 = 5.644 \times 10^3 \frac{d\pi}{\pi^2}\ \text{Hz} \quad \text{at} \quad 100\ \text{MHz} \tag{17}$$

where $d\pi$ is the mean rate of change of horizontal parallax per half day in seconds of arc (tabulated in The American Ephemeris and Nautical Almanac for the appropriate year) and π is the equatorial horizontal parallax in minutes (also tabulated in The American Ephemeris and Nautical Almanac). These formulas are probably accurate to within ±10 Hz for a wave frequency

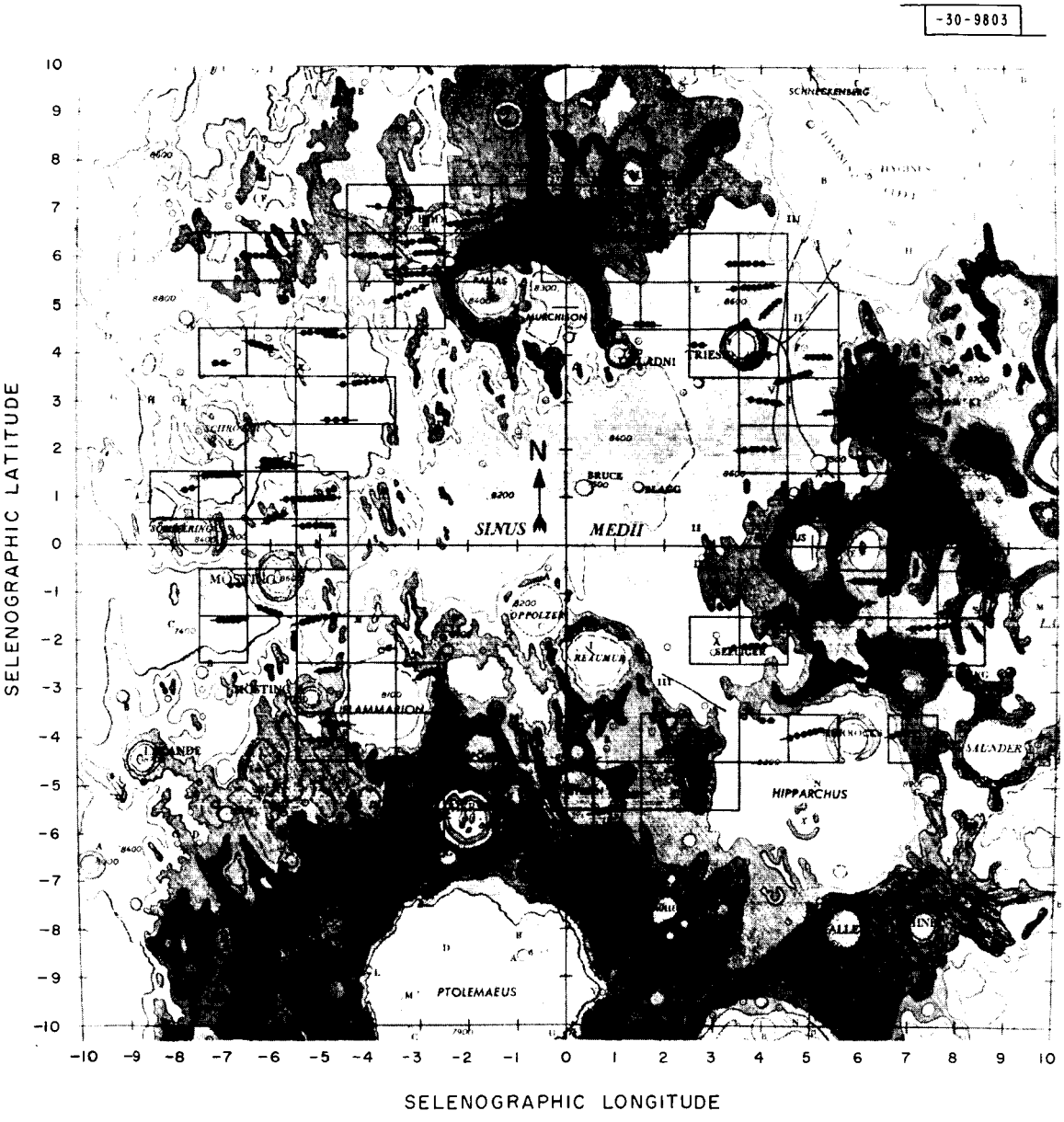

Fig. 5. Topographic map of central portion of lunar surface showing location of subradar points. Because of the moon's libration (Sec. I-C), the subterrestrial point wanders over the lunar surface in the course of a month and approximately describes an ellipse. [After Yaplee, et al. (1964) – official U.S. Navy photograph.]

of 100 MHz. For more precise observations, machine computations are required, and Fricker, et al. (1960) have developed the necessary formulas.

Careful measurements of the Doppler shift of the echoes have been made by Blevis (1957) and by Fricker, et al. (1958) but did not reveal any systematic differences between observed and predicted values. Thomas (1949) considered the possibility that the radius of the earth might be determined from such observations. He concluded that the changes in the position of the effective scattering center of the moon would be sufficient to prevent precise measurement of the Doppler shift. Pettengill (1961) has shown that this can be overcome by employing a coherent pulse radar (Sec. I-H) and resolving the echo into different frequency components. The overall width of this power spectrum will be set by the apparent rotation rate, but by bisecting the spectrum, Pettengill was able to measure mean Doppler shifts to an accuracy of ±0.1 to ±0.2 Hz with a radar operating at 440 MHz.

3. Rotational Effects

The center of the moon's disk as seen from the earth is a point which wanders over the surface. This motion has three principal causes which are illustrated in Fig. 6(a-c). In (a) libration in longitude is seen to result from the fact that because the moon rotates on its own axis with constant angular velocity and moves in an elliptical orbit, it is unable to present exactly the same face to the earth at all times. Thus, if a stick were placed on the surface at perigee pointing toward the earth, it would do so again only at apogee. In between there would be an angle of up to $7\frac{1}{2}^\circ$ between the line of sight to the earth and the stick. The rate of libration ℓ_L introduced by this component is at its maximum near apogee or perigee, when it has a value of about 4×10^{-7} rad/sec. It is direct in sense at apogee and retrograde at perigee. In (b) libration in latitude is shown to result from the fact that the moon's axis of rotation is not perpendicular to the plane of its orbit, but inclined to it by $6\frac{1}{2}^\circ$. This component has a period of one sidereal month and its rate ℓ_B reaches a maximum value of 3×10^{-7} rad/sec when the moon

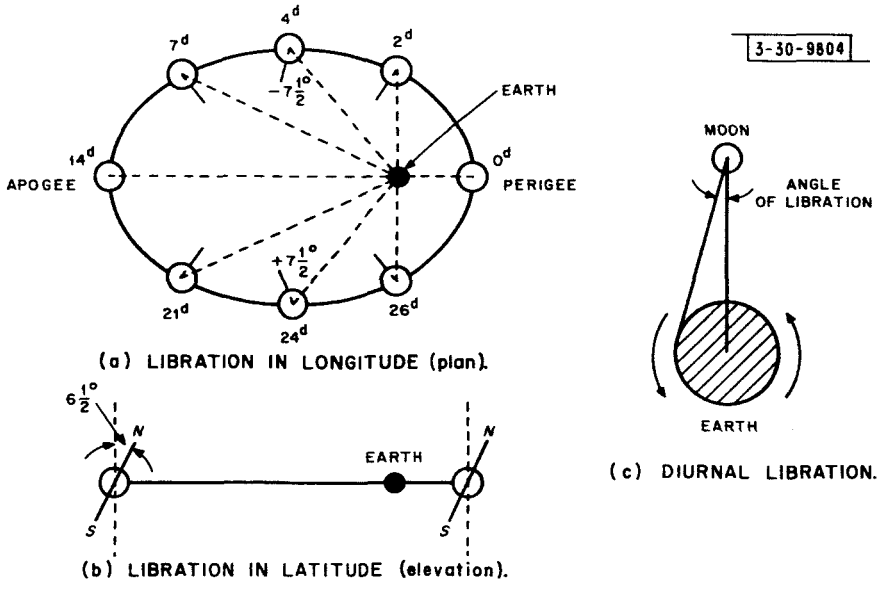

Fig. 6. Three principal causes of moon's libration.

crosses the nodes of its orbit. Finally in (c) the largest component, diurnal libration, is illustrated. An observer on the earth sees a parallactic shift between the center of the moon's disk and the true center of the moon as the earth rotates. This component is direct in sense when the moon is in transit. The rate of diurnal libration ℓ_D reaches a maximum value of $12 \cos\varphi' \times 10^{-7}$ rad/sec at meridian transit when the moon's declination $\delta \simeq 0°$ for an observer at a latitude φ'.

At any instant the moon may be considered to be spinning about an axis with angular velocity defined by the vector addition of the three main components ℓ_D, ℓ_L, and ℓ_B. The values of ℓ_L and ℓ_B are approximately constant over a given day and can be obtained by interpolation from the figures listed in The American Ephemeris and Nautical Almanac for the earth's selenographic longitude and latitude. The total rate of libration ℓ_T may then be computed by resolving ℓ_D, ℓ_L and ℓ_B into components along and perpendicular to the line of sight. The component along the line of sight introduces no range changes and can be ignored. Evans, et al. (1959) used the expression

$$\ell_T^2 = (12 \cos\varphi' \cos HA + \ell_L)^2 + (12 \cos\varphi' \cdot \sin\delta \cdot \sin HA + \ell_B)^2 \text{ rad/sec} \qquad (18)$$

(where HA = hour angle) to compute ℓ_T. This expression was approximately true at the time of their observations, because the moon was at its most northerly declination and is not otherwise valid. For precise calculations, the more complicated formulas developed by Fricker, et al. (1958) should be employed.

Signals which are returned from regions other than those along the apparent axis of librational rotation will exhibit an additional Doppler shift due to the apparent rotation of the moon. The maximum Doppler shift of the signals will occur for reflections from the limb regions most distant from the libration axis and may be expressed as

$$f_o = \pm \frac{2\ell_T a}{\lambda} \qquad (19)$$

where λ is the radio wavelength and a is the lunar radius. Other elements of the lunar surface will introduce a Doppler shift into the signals they reflect which is directly proportional to the distance of the element from the libration axis. Thus the moon's disk may be imagined as ruled by a series of lines all parallel to the libration axis, and each of which represents a locus of constant Doppler shift (Browne, et al., 1956). It follows that if the moon reflects as a uniformly bright scatterer, the RF power spectrum $\overline{P}(f)$ of the echoes will be hemispherical in shape, because the amount of power at each frequency will be proportional to the length of the corresponding strip. For any other scattering law, the echo power spectrum will be modified in a way that depends directly upon the distribution of scattering centers over the visible disk. Figure 7 shows the power spectra $\overline{P}(f)$ expected for both Lommel-Seeliger (Eq. 11) and Lambert (Eq. 12) scattering, assuming that the reflection coefficient is independent of the angle of incidence.

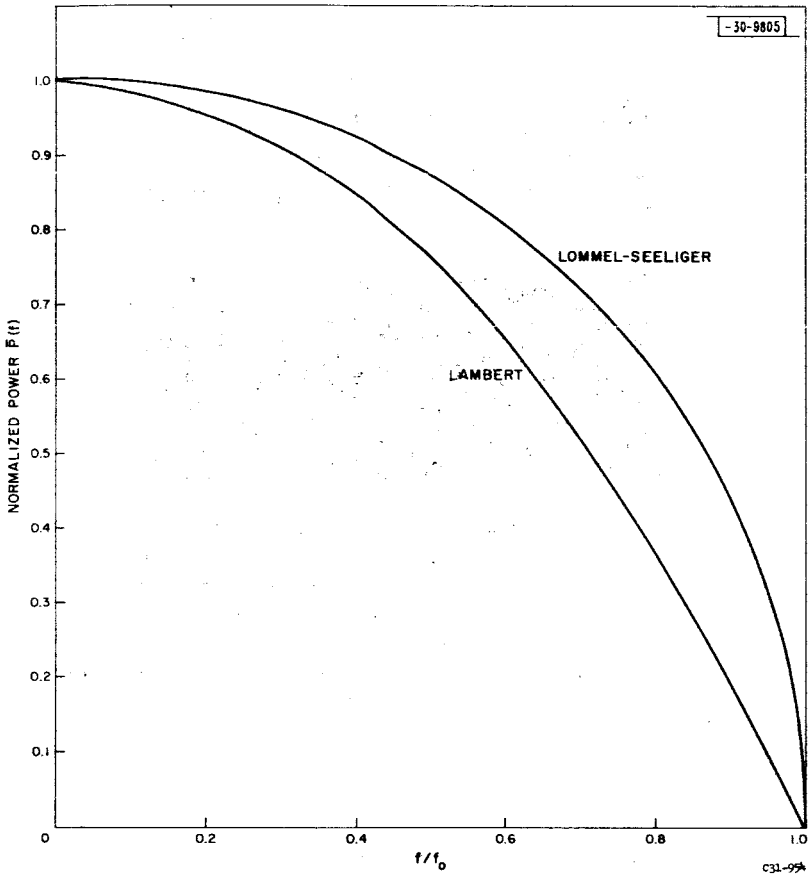

Fig. 7. RF power spectra $\bar{P}(f)$ expected for moon echoes where disk behaves as Lambert or Lommel-Seeliger scatterer. Abscissa has been normalized by dividing by maximum Doppler shift f_o (Eq. 19) and is identical to distance measured along radius perpendicular to libration axis.

D. FADING CHARACTERISTICS

1. Early Observations*

The first radio echoes from the moon were obtained by DeWitt and Stodola in 1946 (DeWitt and Stodola, 1949). These workers observed that the echoes were subject to severe fading and on some days were totally absent. Later Kerr and Shain (1951) recognized that there were two sources of fading: one of ionospheric origin and a second, faster component attributable to the moon itself. These two forms of fading are illustrated in Fig. 8. Murray and Hargreaves (1954) showed that the long period fading was due to the Faraday effect in the earth's ionosphere. Fricker, et al. (1958) and Evans, et al. (1959) demonstrated that this long period fading could be eliminated conveniently by employing circularly polarized waves for transmission and reception. This component depends upon the rate of change of electron content along the line of

* For a historical account, see Evans (1962a).

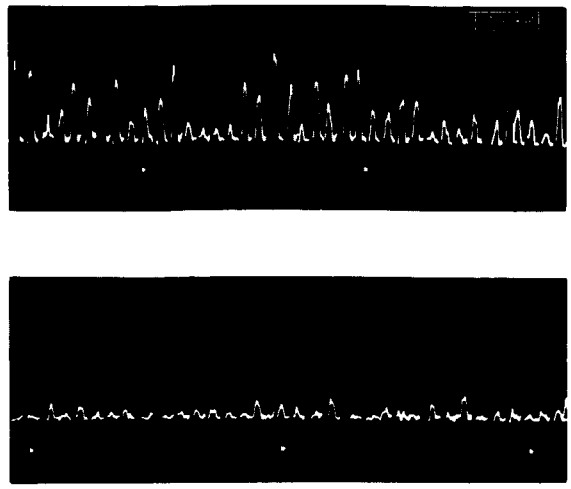

Fig. 8. Two samples of moon echoes observed by Browne, et al. (1956). In each sample, only echoes have been photographed and these occur every 1.8 sec. Dots below traces are half-minute time marks. In both samples, echoes are fading rapidly and this is attributed to moon itself. Echoes in lower sample, which were observed some 14 minutes before those in the upper, are on average much weaker because of rotation of plane of polarization of radio waves in earth's ionosphere (Faraday effect).

sight and varies inversely as the square of the radio-wave frequency. At a frequency of 100 MHz, the interval between maxima or minima in the fades introduced by the Faraday effect is usually longer than about 15 minutes. For most subsequent observations, circular polarization has been employed to eliminate this undesirable effect.

In their article published in 1948, Grieg, et al., pointed out that signals might be received at the earth from two or more "bounce points" and thereby give rise to destructive and constructive interference. The moon does not scintillate when observed optically simply because the sun does not provide a source of coherent radiation as any radar transmitter does. Kerr and Shain (1951) extended this idea to the concept of a very large number of scattering centers distributed over the lunar surface. The rate of fading caused by the moon then depends upon (a) the rate of apparent rotation of the moon ℓ_T and (b) the distribution of these scattering centers. Since (a) is known, (b) can be deduced from observations of the fading rate of the signals. In this section, we outline this earliest method of studying the moon's behavior.

2. Echo Amplitude Statistics

The effect of the librational spin ℓ_T will be to alter the path lengths of the various scattering centers distributed over the surface of the moon, with a consequent change in the phases of all the components of the reflected signal which make up the echo. This will cause the echo amplitude to fluctuate at a rate which will depend upon ℓ_T. The statistical properties of the echo amplitude are of immediate interest. If the number of scattering centers is small (less than 10), it would be possible to infer their number from studies of the echo amplitude distribution. Browne, et al. (1956) reported that the echo amplitude distribution followed the Rayleigh law

$$N_z(dz) = \frac{z}{z_o^2} \exp\left[-\frac{1}{2}\left(\frac{z}{z_o^2}\right)\right] dz \qquad (20)$$

where N_z is the number of echoes in the amplitude range z to z + dz and z_o is the rms echo amplitude. This indicates that the number of scattering centers is numerous (at least greater than 10). Fricker, et al. (1958) observed that the echo amplitude distribution parted from the Rayleigh law in a manner predicted by Rice (1944, 1945) when a steady or nonfading component is present. Further observations by von Biel (1962) indicated a serious departure from the Rayleigh law and a fit to a Rice curve with a parameter a = 1.5. From this, von Biel concluded that over 50 percent of the echo power was provided by a steady or coherent reflector. This must be discounted, however, since the spectrum observations (Sec. I-H) indicate no such large monochromatic component. If a steady component did exist, it might be expected to arise from that part of the lunar surface nearest the earth which conforms to the mean spherical surface. For a completely smooth surface, a system of Fresnel zones can be imagined to exist which determines the intensity of the reflected signal (which, of course, would not fade). If now the surface is made slightly irregular, parts of these Fresnel zones will be removed and an additional "scatter" signal component (Moore and Williams, 1957) will arise from the irregular parts of the surface. The "scatter" component will fade due to constructive and destructive interference.

By using short pulses, it might be possible to restrict the illuminated portion of the lunar surface to that part near the center where any coherent component would be expected to arise. The fraction of the power associated with the "scatter" component would thereby be reduced in comparison with the coherent component. Yaplee, et al. (1959) have studied the fading characteristics of the moon echoes using 2-μsec pulses at 10-cm wavelength. Their results are shown in Fig. 9 and indicate a departure from the Rayleigh law for the leading-edge echo. However, at the leading edge the echo was observed to fade, indicating that a significant scatter component was also present. This is hardly surprising in view of the fact that the first Fresnel zone would have a radius of about 300 m (at 10-cm wavelength) but a 2-μsec pulse would illuminate a region with a radius of the order of 20 km. The results of Yaplee, et al. (1959) may be open to the criticism that the first visible echo on the time base may always have been attributed to the leading edge. If so, the echo amplitude is bound to appear to exhibit less variation than later echoes. Contradictory results have been reported by Hughes (1960) who has repeated Yaplee's measurements and found that the signal showed "no steady component but fluctuates in a random fashion." On the other hand, Mehuron (1963), using a resolution of 3.1 μsec, has found alternate evidence (Sec. I-E-2) for a coherent component which he concludes is responsible for 2.5 percent of the total echo power reflected by the moon. Against this may be set the fact that Mehuron's results were obtained from one small sample of echoes and hence may not be representative.

In conclusion, it seems that at all ranges there is a multiplicity of scattering centers and that a discrete coherent reflector has not yet been completely isolated, possibly because pulses sufficiently short have not been employed. There is conflicting evidence of the presence of a coherent component in the signals reflected from the leading edge. Caution must be used when interpreting the published observations. Relative line-of-sight velocities of the scatterers is a minimum at the center of the disk and the fading rate of signals reflected from this region is

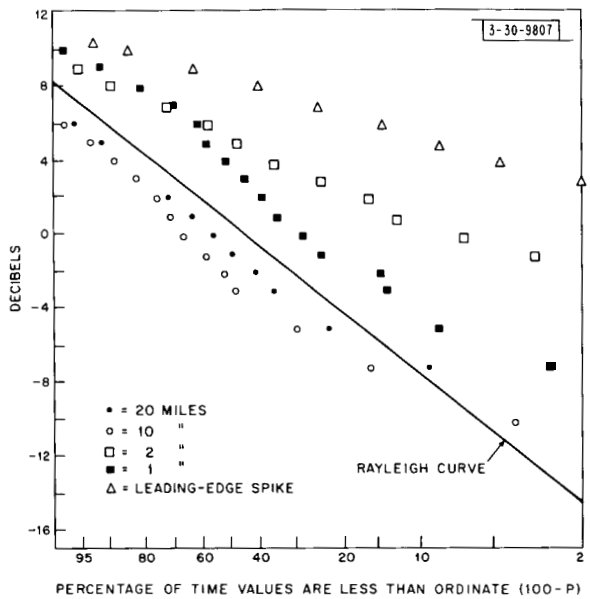

Fig. 9. Statistical properties of echo amplitudes observed by Yaplee, et al. (1959) for moon echoes at different delays with respect to first observable echo. These results suggest that there is a multiplicity of reflecting centers for delay >50 μsec and hence Rayleigh law is observed. For the leading edge, however, there is departure from Rayleigh law indicating presence of nonfading component in the signals. [R.N. Bracewell, Ed., Paris Symposium on Radio Astronomy, Stanford Univ. Press, 1959).

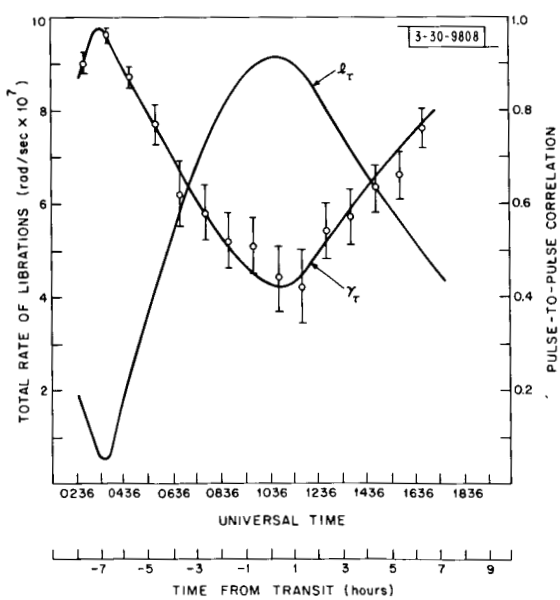

Fig. 10. Correlation between moon echoes transmitted at 1-sec intervals at 100 MHz as observed by Evans, et al. (1959). Also plotted is total libration ℓ_T and it is clear that rapid fading of echoes is directly related to rate of moon's libration.

correspondingly much slower. Thus the time over which the echo amplitude should be studied is considerably longer than for more distant regions. The four-minute sample analyzed by Yaplee, et al. (1959) may have been inadequate. Existence or nonexistence of a coherent component is likely to remain a source of controversy for some time, until measurements are made with better resolution.

3. Echo Autocorrelation

The echo fading rate can be defined by the pulse-to-pulse autocorrelation coefficient $\gamma(\tau)$ given by

$$\gamma(\tau) = \frac{\overline{z(t)\, z(t+\tau)} - \overline{z(t)}^2}{\overline{z^2(t)} - \overline{z(t)}^2} \tag{21}$$

where z(t) denotes the echo amplitude at time t, and $z(t + \tau)$ at a time τ later. In Eq. (21), the "bars" denote averages. The autocorrelation observed at any time will depend upon the rate of libration ℓ_T at that time as demonstrated in Fig. 10. The effect of additive noise will be a reduction of the observed value for $\gamma(\tau)$ below the true value so that for large τ

$$\gamma(\tau)_{\text{true}} = \gamma(\tau)_{\text{observed}} \left[\frac{\overline{P}_s + \overline{P}_n}{\overline{P}_s}\right]^2 \tag{22}$$

where $\overline{P}_s$ is the average power in the signal and $\overline{P}_n$ is that due to noise. The error bars shown in Fig. 10 arise not from noise but from the limited number of pairs n of echoes (at t and $t + \tau$) used in the sample

$$\text{Error} = \pm \frac{1 - [\gamma(\tau)]^2}{\sqrt{n}} \quad . \tag{23}$$

The autocorrelation function of video signals $\gamma(\tau)$ is simply the Fourier cosine transform of the power spectrum of the video signals. Because cross terms are introduced at the detector, the video and RF power spectra are not the same. For a square-law detector, the relation between $\gamma(\tau)$ and the RF power spectrum $\overline{P}(f)\, df$ is given by

$$\gamma(\tau) = \left\{\int_{-\infty}^{+\infty} \overline{P}(f) \cos\left[i2\pi f\tau\right] 2\pi\, df\right\}^2 \quad . \tag{24}$$

That is, the normalized autocorrelation function $\gamma(\tau)$ of the echo amplitude is given by the square of the Fourier cosine transform Ψ of the normalized RF power spectrum $\overline{P}(f)$. This relation (Eq. 24) is strictly valid only where the signal resembles narrow-band Gaussian noise. When this is true and a linear detector is employed, the relationship is more complex but approximates

$$\gamma(\tau) \simeq \frac{16}{17}\left[\Psi^2 + \frac{\Psi^4}{64} + \ldots\right] \quad . \tag{25}$$

Autocorrelation functions of echo amplitude have been determined at 38.25 (Evans and Ingalls, 1962), 100 (Evans, et al., 1959), 120 (Evans, 1957), and 440 MHz (Ingalls, privately communicated). The results for 38.25, 100, and 440 MHz are shown in Fig. 11. The abscissa has

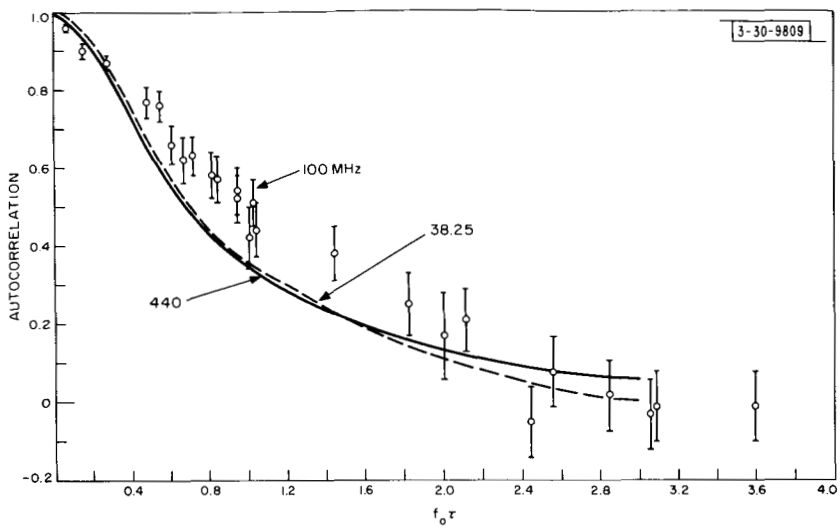

Fig. 11. Echo autocorrelation $\gamma(f_o\tau)$ observed at 38.25 (Evans and Ingalls, 1962), 100 (Evans, et al., 1959) and 440 MHz (Ingalls, privately communicated). Abscissa is time delay τ between two samples of echo multiplied by Doppler shift f_o corresponding to moon's limb in order to remove dependence on libration rate.

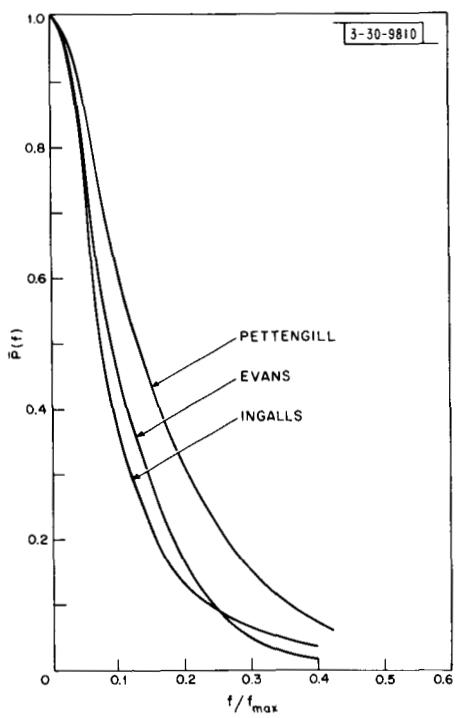

Fig. 12. RF power spectra $\bar{P}(f)$ obtained for moon echoes by Fourier transformation of autocorrelation curves $\gamma(f_o\tau)$ presented in Fig. 11. Difference between those marked "Evans" and "Ingalls" is not considered significant. Curve marked "Pettengill" has been obtained by appropriate numerical integration of angular law $P(\phi) \propto \exp(-10 \sin\phi)$ published by Pettengill and Henry (1962a). Broader spectrum produced in this way is thought to indicate that the law $\exp(-10 \sin\phi)$ does not accurately indicate angular dependence.

been normalized by multiplying the time delay τ by the maximum Doppler shift f_o (Eq. 19) to remove the dependence of the results on the rate of libration ℓ_T (Fig. 10). The difference between the 100 MHz results and those at the two other frequencies is in part probably a consequence of inaccuracies in the value for f_o introduced by employing Eq. (18) to compute ℓ_T. By employing the reverse of the transform given in Eq. (24), the power spectra $\overline{P}(f)$ shown in Fig. 12 were obtained. It is evident from these spectra that the bulk of the echo power is returned from the central portion of the moon's visible disk.

At a frequency of 100 MHz, f_o is usually less than ±2 Hz. Consequently, it would be exceedingly difficult to obtain these spectra with a conventional narrow-band receiver employed as a spectrum analyzer.* By employing coherent processing (Sec. I-H), it is possible to obtain more detailed spectra in which the two halves are maintained separately. In Fig. 12, the two halves of the spectra have been added as a consequence of the removal (by the detector) of the information contained in the phase of the signals. In actual practice, short pulse measurements have proved a more useful means of studying the lunar scattering for three reasons: (a) there is a direct relationship between echo power vs angle (i.e., the angular power spectrum) and the echo power vs delay, but not the echo power spectrum, (b) the resolution obtainable in delay is usually much finer than that in frequency, and (c) it is often easier to handle a large dynamic range for signals separated in delay, but not in frequency. We discuss next the echo power vs delay measurements.

E. ECHO POWER VS DELAY

1. Early Observations

Kerr and Shain (1951) were the first to attempt short pulse observations of the moon in order to see if the pulses were lengthened by the distribution of the scattering centers in depth. They reported that 1-msec pulses were lengthened in support of their conclusion (obtained from autocorrelation measurements) that the moon was approximately a uniformly bright reflector. Evans (1957), using 2-msec pulses, reached the reverse conclusion in support of his observation (also from autocorrelation measurements) that the moon was, in fact, a limb-dark scatterer. Immediately on publication of these later results, the work performed several years previously at the Naval Research Laboratory was released (Trexler, 1958). Trexler employed a radar operating at 198 MHz with a pulse length of 12 μsec and Fig. 13 illustrates the range display observed in this work. Some 50 percent of the echo power was returned within the first 50 μsec of the pulse. This result agrees well with the power spectrum measurements described in the previous section. The exponential tail of the echo appeared to extend some 500 μsec beyond the leading edge of the echo, but this appeared to be a function of signal-to-noise ratio. Yaplee, et al. (1958) and later Hey and Hughes (1959) reported similar behavior at a wavelength of 10 cm, when 2- and 5-μsec pulses were used.

The difficulty involved in these observations is to obtain good range resolution together with adequate signal-to-noise ratio. To achieve good range resolution, one is obliged to use short

* This was attempted by Fricker, et al. (1958).

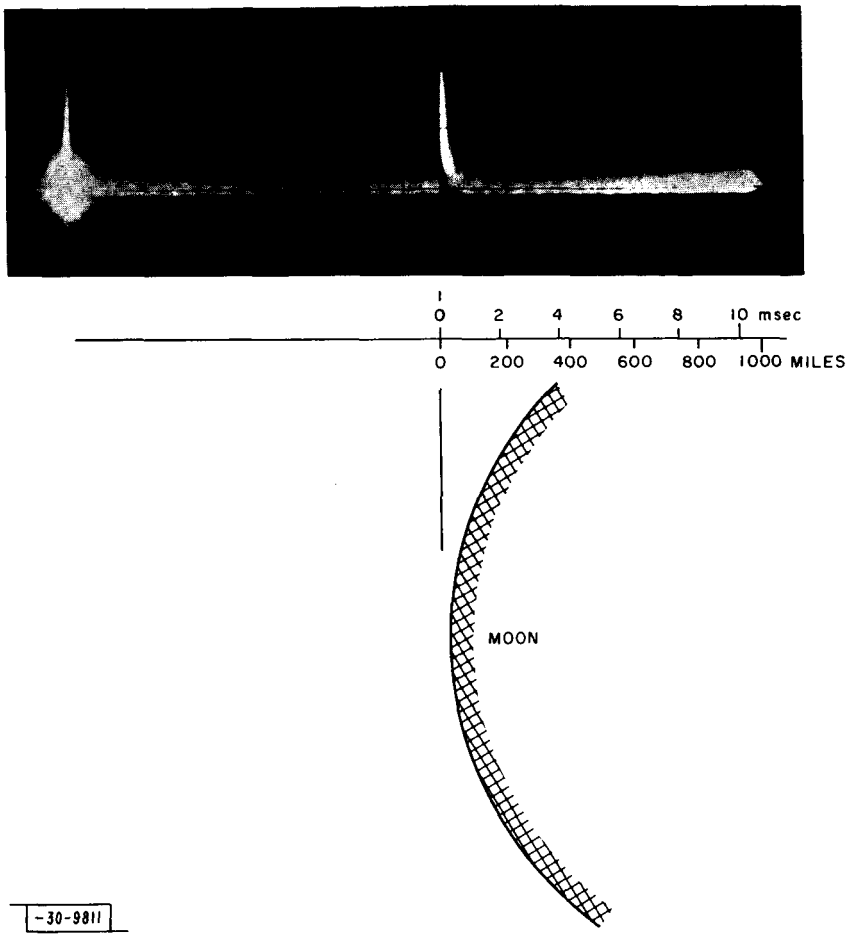

Fig. 13. Moon echoes observed by Trexler (1958) compared to scale with curvature of moon.

pulses. The peak echo power thus falls, owing to a reduction in the illuminated surface area (Fig. 1). Further, the receiver bandwidth must be adjusted to match the pulse length, thereby making the receiver admit more noise power as the pulse is shortened. Thus the signal-to-noise ratio falls rapidly as the pulse length is reduced, and even at the present time short pulse observations have been made only at a limited number of wavelengths, though the total cross section has been measured at many. The observations of Trexler, Yaplee, et al., and Hey and Hughes indicated that echoes come only from a portion of the surface near the center of the disk. This proved to be a consequence of the limited sensitivity of their equipment. Pettengill (1960) and Leadabrand, et al. (1960) showed that echoes could be measured all the way out to the limbs with a sufficiently powerful radar system.

The first truly quantitative measurements of echo power vs delay from the leading edge to the limb were performed by Pettengill and Henry (1962a) at a wavelength of 68 cm using 65-μsec pulses. They employed a digital computer to average the echo intensity at range intervals of 250 μsec. By repeating the observations when the moon was at slightly different ranges, Pettengill and Henry were able to achieve a resolution substantially better than 250 μsec as shown in Fig. 14.

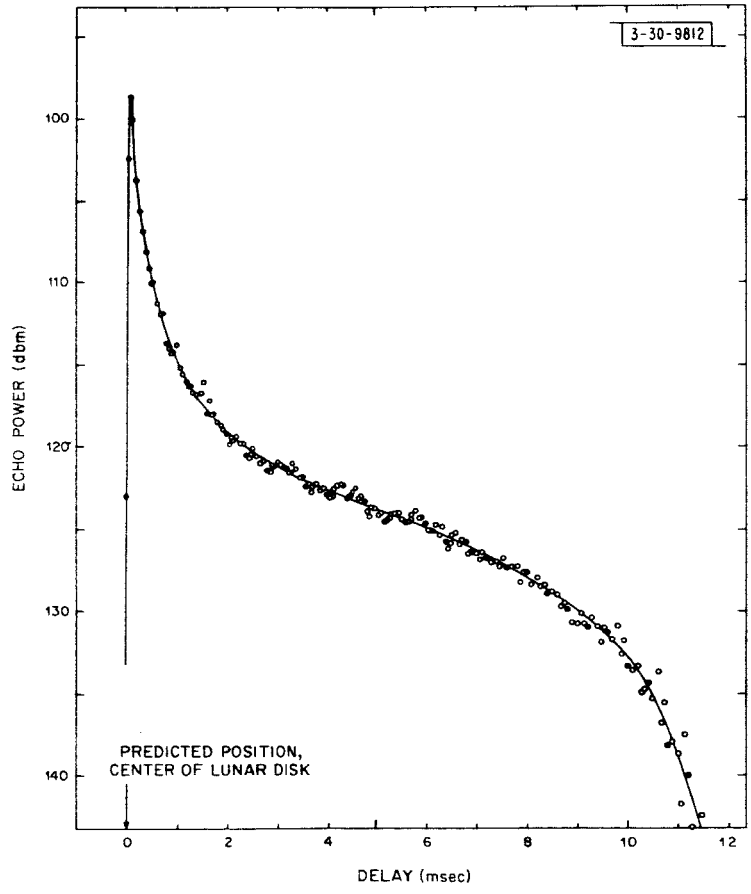

Fig. 14. Distribution of echo power with range P(t) observed at 68-cm wavelength using transmitter pulse length of 65 μsec (18 July 1960).

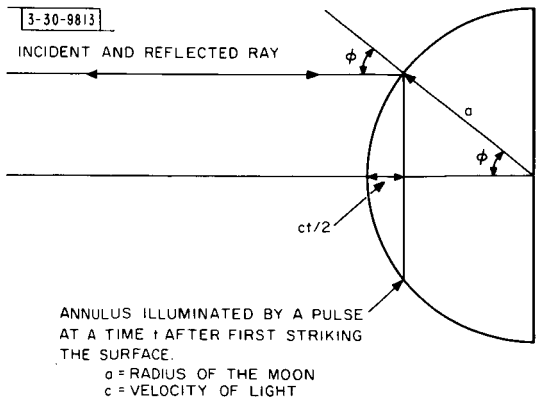

Fig. 15. Relation between range delay t and angle of incidence and reflection ϕ of radio waves.

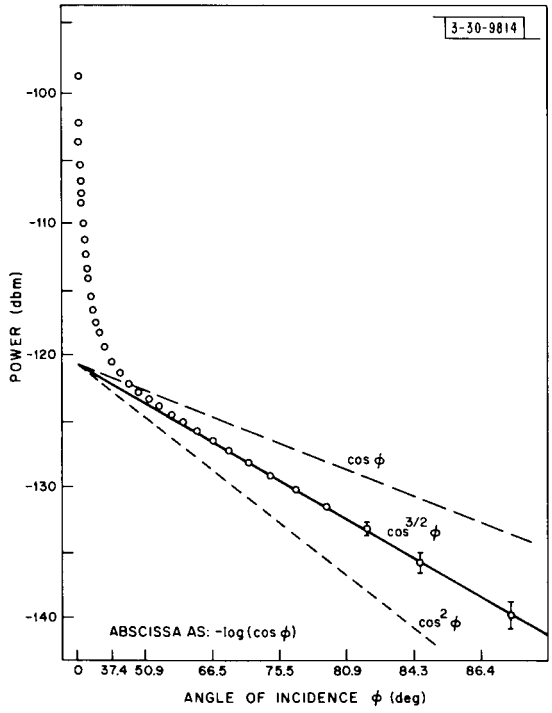

Fig. 16. Angular power spectrum $\bar{P}(\phi)$ obtained from echo power distribution in Fig. 14. Lambert ($\cos^2\phi$) and Lommel-Seeliger or uniformly bright behavior ($\cos\phi$) are shown for comparison.

There is a direct relationship between the delay t and the angle φ which the ray makes to the normal to the surface as illustrated in Fig. 15. Thus the abscissa of Fig. 14 can be transformed to one involving φ in order to determine the dependence of the echo power $\overline{P}(\varphi)$ on the angle of incidence and reflection. By taking this step, one is in fact assuming that the surface has everywhere the same statistical properties. This is certainly open to question, particularly for very short pulses where the resolution is high. However, if the surface is statistically uniform, the plot $\overline{P}(\varphi)$ obtained is simply the angular scattering law $\sigma_o(\varphi)$ defined previously (in Fig. 2). To make it clear that an assumption is involved here, we shall use the symbol $\overline{P}(\varphi)$ to denote the angular dependence obtained from short pulse measurements. In the limit, where very short pulses τ are used (as $\tau \to 0$) to observe a statistically uniform sphere, $\overline{P}(\varphi) \to \sigma_o(\varphi)$.

When Pettengill and Henry (1962a) plotted the echo power as a function of log $\cos\varphi$, they obtained Fig. 16 which shows that for $\varphi \geqslant 45°$

$$\overline{P}(\varphi) \propto \cos^{3/2}\varphi \quad . \tag{26}$$

A short pulse τ illuminates an equal amount of area ($\pi ac\tau$) at all delays t but the amount of projected area falls as $\cos\varphi$. Since this effect has not been allowed for, Eq. (26) indicates that the regions where $\varphi \geqslant 45°$ scatter according to a law that lies midway between the Lommel-Seeliger photometric function (uniformly bright) and the Lambert photometric function (slightly limb dark). The scatterers in this region are apparently insensitive to the angles of incidence and reflection, whereas for $\varphi < 45°$ the echo power falls rapidly. Accordingly, Pettengill and Henry (1962a) presumed that there are two different types of scatterer on the lunar surface and termed those responsible for Eq. (26) "diffuse."

When the diffuse component obeying the $\cos^{3/2}\varphi$ law has been subtracted, the remainder represents the power attributable to the central portions of the lunar surface. The marked dependence of this component upon the angle of incidence and reflection φ caused Evans (1957, 1962a), Pettengill (1960), Pettengill and Henry (1962a) to describe it as a "specular" component. This term has given rise to some confusion and since it was not intended to convey that the moon is perfectly smooth, we shall here use the term "quasi specular."

Pettengill and Henry (1962a) observed that this component of the power conformed to the empirical law

$$\overline{P}(\varphi) \propto \exp(-10.5 \sin\varphi) \quad , \quad 7.5° < \varphi < 60° \quad . \tag{27}$$

Meanwhile, Hughes (1960, 1961) had observed that, at a 10-cm wavelength,

$$\overline{P}(\varphi) \propto \exp(-10.2\,\varphi) \quad , \quad 3° < \varphi < 14° \quad . \tag{28}$$

This result was obtained by using 5-μsec pulses and averaging the echo power by means of a single channel analog integrator with a resolution of 20 μsec. Hughes was unable to observe echoes beyond a 1-msec delay and hence could not verify the existence of the diffuse component (Eq. 26) observed by Pettengill and Henry (1962a). Partly on the basis of the similarity of Eqs. (27) and (28), Hughes (1961) concluded that the radio-wave scattering properties of the moon were independent of the radio wavelength λ. Observations at any one wavelength are probably insensitive to structure which has horizontal and vertical scales of less than $\lambda/8$. As the

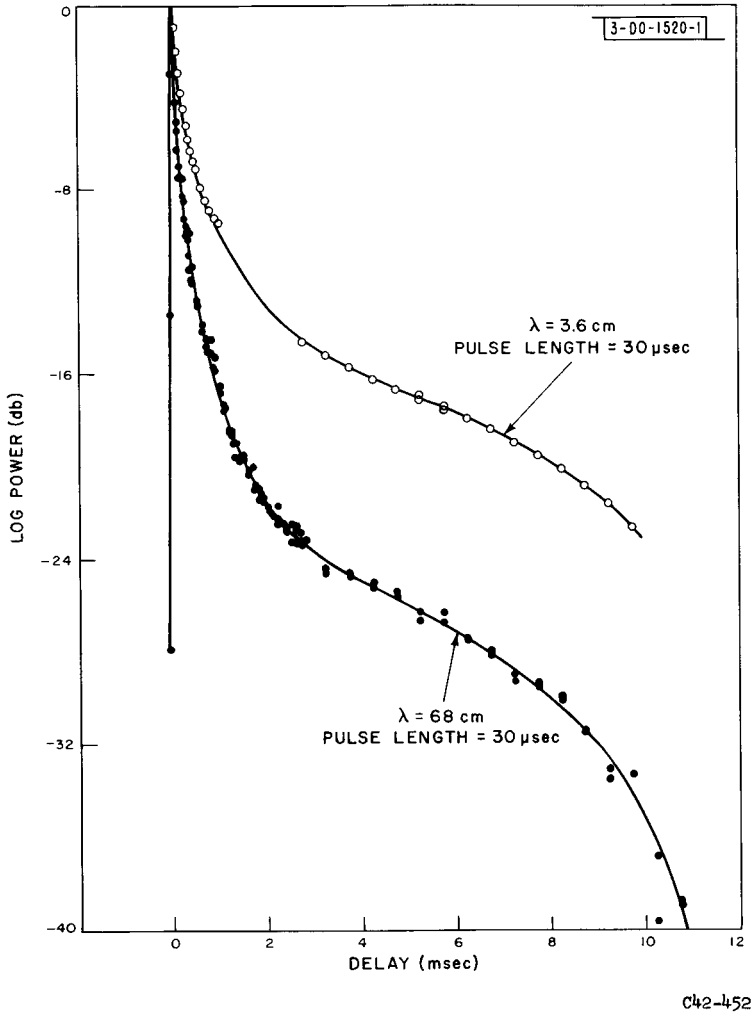

Fig. 17. Average echo power reflected by moon P(t) as a function of delay measured with respect to point closest to radar. The 68-cm results were obtained using same methods of averaging as were employed to obtain 3.6-cm results. Curves have been normalized at zero delay.

wavelength is reduced, the effect of small-scale irregularities should become more serious. Hughes' conclusion, therefore, implies an absence of structure on the lunar surface with a size of the order of 10 cm.

In reaching the conclusion that there was no wavelength dependence, Hughes (1961) ignored the fact that the resolution in the two sets of measurements was considerably different. Evans and Pettengill (1963b) showed that the law given in Eq. (27) when transformed to give the expected power spectrum $\overline{P}(f)$ (Fig. 12) produced a spectrum which was broader than that obtained from the autocorrelation result. They inferred from this that for $\lambda = 68$ cm, $\overline{P}(\varphi)$ falls more rapidly than $\exp(-10.5 \sin\varphi)$, and this was subsequently shown to be the case.

2. Recent Observations

A search for a wavelength dependence in the scattering was undertaken by Evans (1962b, c). A 48-channel integrator was constructed and first employed with a 30-μsec pulse radar operating at 3.6 cm. For reception, the resolution in delay was 20 μsec. Later the measurements were repeated at 68-cm wavelength with the same pulse length and resolution in delay. The two sets of measurements are compared in Fig. 17. A clear change in $\overline{P}(t)$ is evident. At the shorter wavelength, the leading-edge echo is not so prominent as at 68 cm. The laws representing the component from the leading edge (after subtracting the diffuse component) were observed to be

$$\text{at } 68 \text{ cm} \quad , \quad \overline{P}(\varphi) \propto \exp(-12.5 \sin\varphi) \quad , \quad 5° < \varphi < 12° \tag{29}$$

$$\text{at } 3.6 \text{ cm} \quad , \quad \overline{P}(\varphi) \propto \exp(-7.1 \sin\varphi) \quad , \quad 5° < \varphi < 18° \quad . \tag{30}$$

The measurements at 68 cm were then repeated with 12-μsec pulses and 10-μsec resolution in delay to achieve an over-all resolution comparable to that of Hughes (1961). A comparison of these 68- and 10-cm results is given in Fig. 18. The leading-edge or "quasi specular" components were now represented by the laws

$$\text{at } 68 \text{ cm} \quad , \quad \overline{P}(\varphi) \propto \exp(-15.3 \sin\varphi) \quad , \quad 3° < \varphi < 14° \quad . \tag{31}$$

$$\text{at } 10 \text{ cm (Hughes, 1961)} \quad , \quad \overline{P}(\varphi) \propto \exp(-10.2\,\varphi) \quad , \quad 3° < \varphi < 14° \quad . \tag{32}$$

Evidently, there is a progressive wavelength dependence from 3.6 to 68 cm and this can be masked where observations achieving very different amounts of resolution in delay are compared.

Evans and Hagfors (at this Laboratory) repeated these measurements at a wavelength of 23 cm and observed that the scattering curve at this wavelength lies (as expected) between the curves for $\lambda = 68$ cm and $\lambda = 10$ cm. The results of the observations of P(t) performed at Lincoln Laboratory are summarized in Table III.

At longer wavelengths ($\lambda = 7.84$ m), Evans and Ingalls (1962) found that the echo power spectrum was indistinguishable from that observed at $\lambda = 68$ cm (Fig. 11). However, Faraday fading of the echoes and ionospheric scintillation both seemed to have been present and may have introduced considerable error. Davis and Rohlfs (1964) have employed a 250-μsec pulse radar at an 11.3-m wavelength to obtain the scattering behavior over the first 4 msec of delay. Despite the long pulse used, they found (Fig. 19) that the wavelength dependence continued in the meterwave region. Because ionospheric scintillation effects cannot introduce systematic errors in short pulse determinations of the scattering behavior, this seems to be the only reliable technique at these long wavelengths.

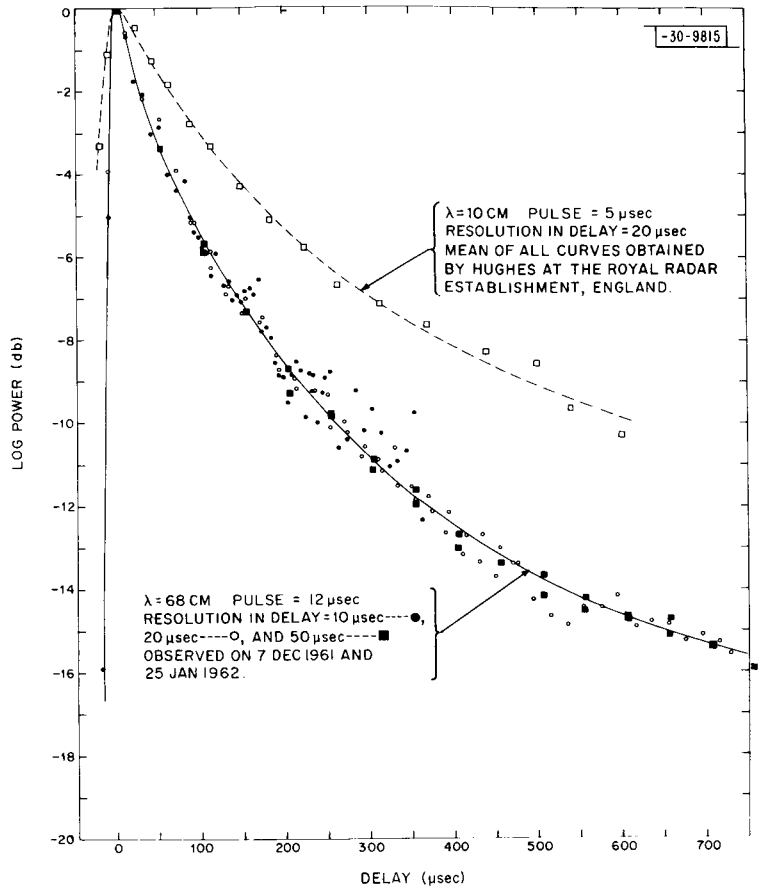

Fig. 18. High resolution measurements of P(t) at 68- and 10-cm wavelengths (Hughes, 1961). As in Fig. 17, clear wavelength dependence can be observed. Curves have been normalized at zero delay.

TABLE III

LINCOLN LABORATORY MOON RADAR RESULTS FOR $\bar{P}(t)$

Delay (t) (μsec)	φ°	λ = 3.6 cm*	23 cm†	68 cm‡ (db)	Delay (t) (msec)	φ°	λ = 3.6 cm	23 cm	68 cm (db)
10	2.38	0	0	0	2.0	34.16	−12.9	−18.65	−21.8
20	3.37	−0.1	−0.85	−0.6	2.25	36.30	−13.5	−19.1	−22.3
30	4.11	−0.4	−1.40	−1.5	2.50	38.33	−14.0	−19.55	−22.7
40	4.77	−0.55	−1.9	−2.2	2.75	40.28	−14.35	−19.85	−23.1
50	5.31	−0.85	−2.35	−2.8	3.0	42.16	−14.85	−20.2	−23.5
60	5.83	−1.05	−2.75	−3.3	3.25	43.97	−15.1	−20.5	−23.8
70	6.30	−1.35	−3.15	−3.8	3.50	45.72	−15.4	−20.85	−24.1
80	6.73	−1.5	−3.55	−4.3	3.75	47.42	−15.7	−21.15	−24.3
90	7.13	−1.75	−3.95	−4.8	4.0	49.08	−15.9	−21.4	−24.5
100	7.53	−1.95	−4.3	−5.2	4.25	50.69	−16.1	−21.7	−24.7
125	8.42	−2.5	−5.05	−6.2	4.50	52.27	−16.35	−21.95	−24.9
150	9.22	−2.9	−5.8	−7.0	4.75	53.82	−16.5	−22.35	−25.1
175	9.96	−3.4	−6.45	−7.7	5.0	55.33	−16.7	−22.5	−25.35
200	10.65	−3.8	−7.0	−8.4	5.25	56.82	−16.9	−22.75	−25.6
225	11.30	−4.15	−7.5	−9.0	5.50	58.29	−17.1	−23.05	−25.9
250	11.92	−4.45	−8.0	−9.7	5.75	59.72	−17.35	−23.3	−26.15
275	12.50	−4.85	−8.45	−10.15	6.0	60.95	−17.6	−23.6	−26.45
300	13.06	−5.15	−8.85	−10.7	6.25	62.55	−17.85	−23.85	−26.8
325	13.60	−5.45	−9.2	−11.1	6.50	63.93	−18.1	−24.2	−27.15
350	14.11	−5.75	−9.55	−11.6	6.75	65.36	−18.35	−24.55	−27.5
375	14.60	−6.0	−9.9	−11.9	7.0	66.65	−18.6	−24.95	−27.85
400	15.09	−6.15	−10.2	−12.35	7.25	67.98	−18.9	−25.35	−28.25
425	15.56	−6.5	−10.5	−12.7	7.50	69.31	−19.2	−25.8	−28.65
450	16.01	−6.70	−10.8	−13.0	7.75	70.63	−19.45	−26.2	−29.0
475	16.45	−7.0	−11.2	−13.3	8.0	71.94	−19.75	−26.65	−29.45
500	16.88	−7.15	−11.35	−13.6	8.25	73.23	−20.1	−27.1	−29.95
600	18.51	−7.9	−12.3	−14.6	8.50	74.53	−20.4	−27.6	−30.45
700	20.01	−8.5	−13.2	−15.4	8.75	75.79	−20.8	−28.15	−30.95
800	21.40	−9.1	−14.0	−16.2	9.0	77.06	−21.2	−28.7	−31.5
900	22.72	−9.55	−14.06	−16.9	9.25	78.33	−21.6	−29.3	−32.1
1000	23.96	−9.9	−15.35	−17.6	9.50	79.59	−22.1	−29.95	−32.75
1100	25.16	−10.3	−15.95	−18.25	9.75	80.84	−22.6	−30.6	−33.35
1200	26.29	−10.7	−16.4	−18.9	10.0	82.09	−23.1	−31.35	−34.05
1300	27.39	−11.0	−16.8	−19.5	10.25	83.34	↑	−32.2	−34.9
1400	28.44	−11.3	−17.15	−20.0	10.50	84.58		−33.25	−35.9
1500	29.42	−11.6	−17.45	−20.4	10.75	85.82	Not	−34.35	−36.9
					11.0	87.06	Measured	−35.85	−38.35
					11.25	88.29		−37.7	−40.1
					11.50	89.53	↓	−40.35	−42.7

	Pulse (μsec)	Delay Resolution (μsec)
*	30	20
†	10	10
‡	12	10

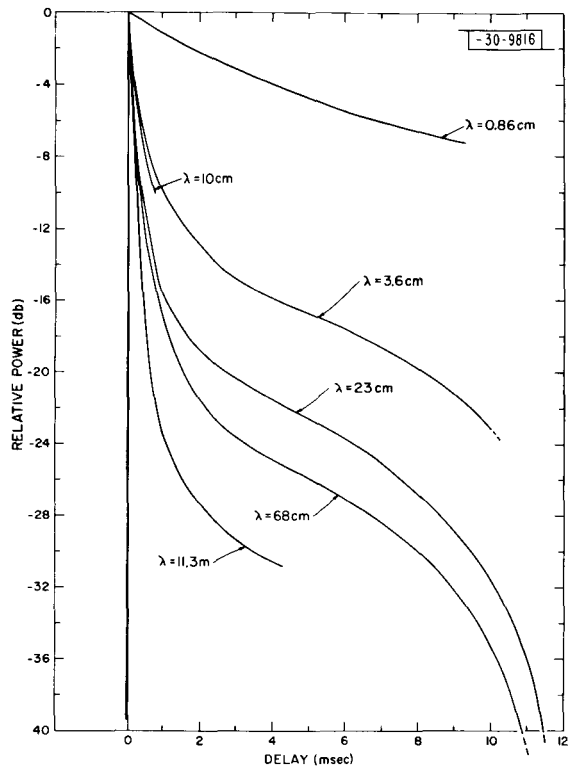

Fig. 19. Results obtained by Davis and Rohlfs (1964) at 11.3-m wavelength using 250-μsec pulses are shown here with the results obtained at 8.6-mm wavelength (Lynn, et al., 1963). The 3.6-, 10-, 23-, and 68-cm results have been included for comparison.

At shorter wavelengths, Lynn, et al. (1963) have determined the scattering behavior at 8.6 mm. These observations were remarkable in that a transmitter power of only 12 watts was employed and that resolution of different range delays was achieved solely by means of the angular resolution afforded by the antenna beam (4.3 min arc). Thus the antenna was directed at different distances from the center of the lunar disk to determine the brightness distribution. This achieves poor range resolution at the limbs but does provide illumination of equal projected areas as distinct from the equal surface area illuminated by short pulse radars. To correct the observations at the limb for the amount of the antenna pattern projected onto the sky which provided no illumination of the moon, Lynn, et al. (1963) assumed that the moon behaved as a uniformly bright reflector (Lommel-Seeliger law). Figure 19 shows their results plotted in the same form as those of Evans and Pettengill (1963c). The wavelength dependence of the scattering of electromagnetic waves by the moon in the range 11 meters to 8 mm is very evident. At 8 mm, only a small highlight appears at the center. The brightness there exceeds that of other regions only by a factor of two. At 3.6 cm, this ratio is of the order of 25 and at 68 cm, it is 150. Lynn, et al. (1963) also reported that there were no differences between the brightness of the maria and the highlands larger than ±2 db – the accuracy of their observations. It would seem that the rough structure responsible for diffuse scattering at 8.6 mm is to be found overlying highlands and maria equally. It is tempting to conclude that the microrelief responsible for the moon's photometric properties also controls the scattering at 8.6 mm – perhaps by extending in depth to several millimeters.

Figure 19 represents a composite plot of all the known published results. It should be pointed out, however, that the experimental resolution differed considerably so that the behavior near $\varphi = 0°$ has been explored well in some cases and poorly in others. Even in the best cases (λ = 10, 23, and 68 cm), the behavior in the region $\varphi < 3°$ has not been explored.

Mehuron (1963) has reported that the echo power represented in Eqs. (27), (29), and (31) for a 68-cm wavelength consists of two components which could be resolved when pulses of 1.8-μsec duration and a resolution in delay of 3.1 μsec were employed. Mehuron associated an initial spike observable over the first ten or so microseconds with a coherent return. The remaining portion of the echo (out to 550 μsec) he ascribed to "quasi specular" scattering (Evans and Pettengill, 1963c). If this interpretation is correct, one would expect to see hourly or day-to-day changes in the relative amplitudes of the two components as the subradar point wanders over the surface of the moon. Unfortunately, only a small sample of data was examined in Mehuron's work. The change in echo power $\overline{P}(\varphi)$ as $\varphi \to 0°$ is so marked that in order to explore it properly, one would require an extraordinarily high-powered radar operating with pulses as short as one-quarter microsecond or less.

We may summarize these results as follows. At radio wavelengths of 1 m and longer, the moon scatters predominantly from those regions at the center of the visible disk which are nearly normal to the line of sight. This suggests a rather smooth surface. However, as the wavelength is reduced, more and more power is returned from other regions, showing that as the scale of the exploring wave is reduced, the surface becomes increasingly rough. At 1-cm wavelength, the disk appears to be almost uniformly bright, indicating that the surface is now essentially covered with structure having dimensions comparable with the wavelength.

3. Depolarized Component

Browne, et al. (1956) observed that the nulls introduced by the Faraday fading were quite deep and that the amount of depolarized power was about 10 percent. This was later confirmed by Blevis and Chapman (1960). Senior and Siegel (1960) were the first to argue that this result alone demonstrates that the reflection occurs from largely smooth surfaces. In order to study the depolarizing ability of the lunar surface, it is desirable to overcome the Faraday fading and this is most easily accomplished by using circularly polarized waves, and receiving the same sense as that transmitted. This experiment was performed at 68-cm wavelength by Pettengill and Henry (1962a) using 400-μsec pulses and later by Evans (1962c) using 200-μsec pulses. As may be seen in Fig. 20, the depolarized component of the power obeys the law $\overline{P}(\varphi) \propto \cos\varphi$, indicating that these signals are scattered equally from all parts of the project disk. The percentage polarization can be expressed in the form

$$\text{Polarization} = \frac{\overline{P}(t) - \overline{D}(t)}{\overline{P}(t) + \overline{D}(t)} \times 100 \text{ percent} \tag{33}$$

where $\overline{P}(t)$ is the average polarized or expected return (Fig. 14) and $\overline{D}(t)$ is the depolarized component (Fig. 20). The percentage polarization has been plotted in Fig. 21, for both the 400- and 200-μsec pulse observations. It appears that the percentage polarization falls linearly out to a delay of 3 msec where it has a value of 60 percent. Beyond this value of delay, the depolarization falls less rapidly and the ratio of the amount of power in the two components $\overline{P}(t)/\overline{D}(t)$ is

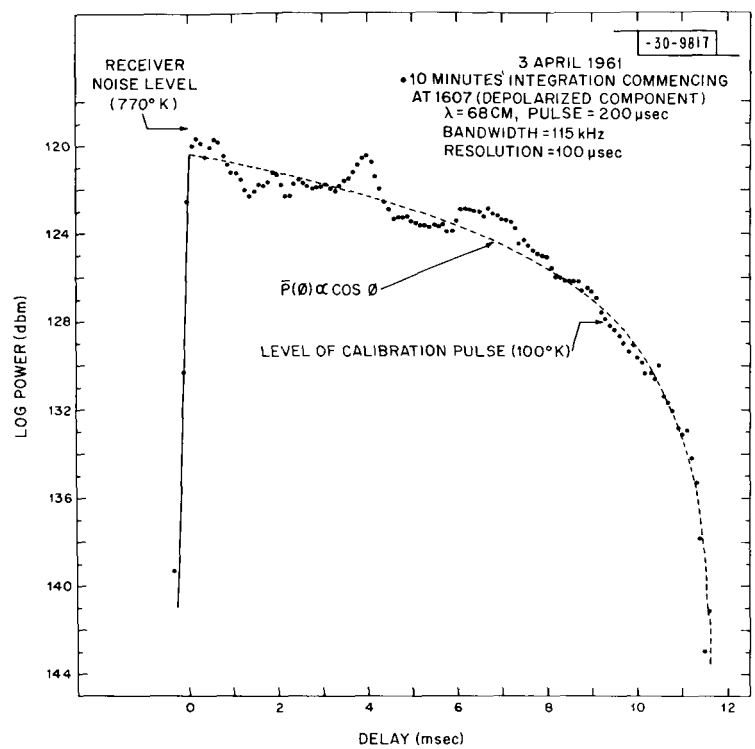

Fig. 20. Average echo intensity vs range delay $\bar{D}(t)$ for depolarized component of signals. Dotted curve indicates expected behavior for a uniformly bright moon. Departures from smooth curve are thought to represent existence of departures from statistical uniformity of surface features over moon's disk. These might be expected to be seen more easily in the depolarized than in the polarized component.

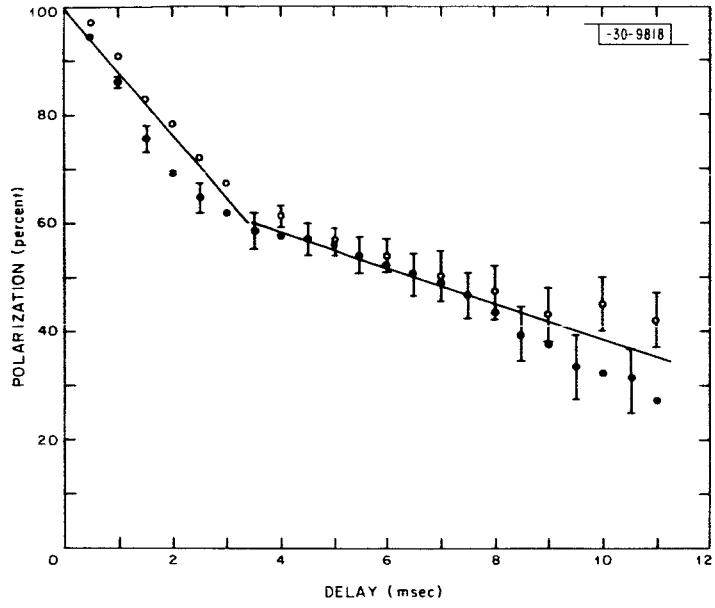

Fig. 21. Percentage polarization of moon echoes as a function of range delay observed at 68-cm wavelength. Values indicated by open circles were computed from the results shown in Fig. 20 by means of expression (33). Earlier values obtained by Pettengill and Henry (1962a) are shown as closed circles.

approximately constant at 3:1. These observations have recently been repeated at 23-cm wavelength with essentially identical results.

Two mechanisms which could give rise to depolarization are (a) multiple reflections on or beneath the surface, and (b) the excitation of surface elements which are comparable in size to the wavelength and re-radiate as dipoles. Probably both mechanisms contribute to some extent, but (a) seems incapable of converting one-quarter of the incident power into the depolarized component.

The similarity of the distribution of the diffuse component of the echo power with delay and the depolarized component suggests that both may be attributed to the same type of scatterer. Small-scale structure on the surface having radii of curvature comparable with the wavelength might be expected to behave largely as isotropic scatterers, and might also be expected to cause some depolarization. We cannot, however, model the scatterers responsible for the diffuse component as a random collection of dipoles, since these would reflect orthogonal circular components of equal intensity. A better model is a mixture of dipoles (responsible for the depolarization) and flat facets (which cause none). Thus the polarization experiment reported here strengthens the case for treating the quasi-specular and diffuse components as separate. Further polarization studies presented in Sec. I-J indicate that much of the small-scale structure that is responsible for the diffuse component of the echo appears to lie beneath the surface; hence, its exact nature is unknown at the present time.

4. Angular Power Spectra

Evans and Pettengill (1963c) have explored a number of empirical laws by which to represent the angular power spectra $\overline{P}(\varphi)$ of the signals. In this section, we briefly review this work.

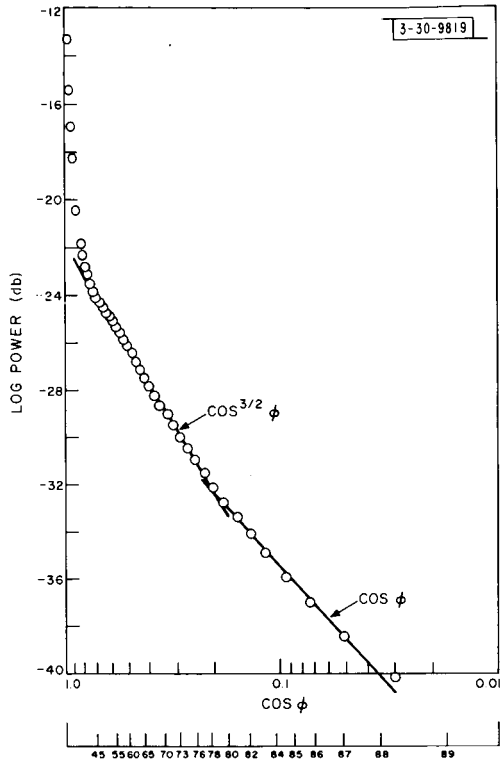

Fig. 22. Average echo power $\bar{P}(\phi)$ plotted as a function of log cos ϕ for observations at 68-cm wavelength with 12-μsec pulses (25 January 1961).

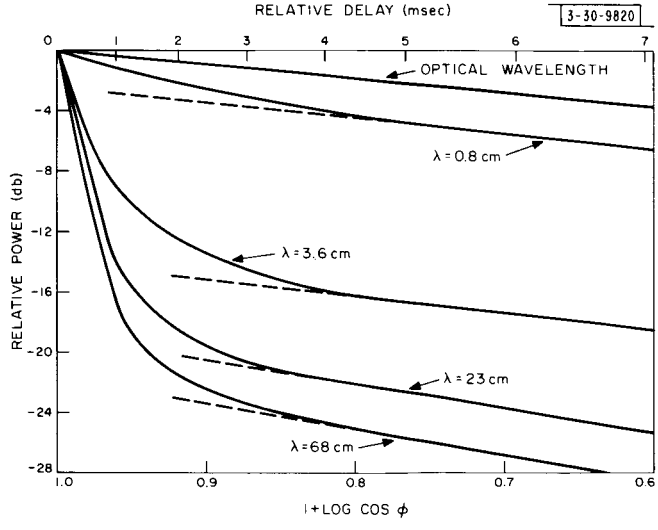

Fig. 23. This plot shows all short pulse observations where diffuse component of echoes could be observed. At 0.86- and 3.6-cm wavelengths this component appears to conform to cos ϕ law and at 23- and 68-cm wavelengths to $\cos^{3/2} \phi$.

The experimental uncertainties in the measurements made to date are least in those for the 23- and 68-cm wavelengths. At 68 cm, Evans (1962c) confirmed that the limb region scattered according to the law $\overline{P} \propto \cos^{3/2} \varphi$ observed by Pettengill and Henry (1962a). In addition, it appeared that when 12-μsec pulses were employed, the region $\varphi > 80°$ conformed to the Lommel-Seeliger law $\overline{P}(\varphi) \propto \cos \varphi$. This behavior is shown in Fig. 22, and has since been found to hold at a wavelength of 23 cm. The uniformly bright behavior for $\varphi > 80°$ at 68 cm was observed at 3.6-cm wavelength for the range $45° < \varphi < 80°$. At 8.6 mm, this law appears to hold for $\varphi > 50°$, though the reliability of this last result may be questioned since it depends on only two points (Lynn, et al., 1963). Figure 23 shows the echo power observed at these four wavelengths plotted as a function of $1 + \log \cos \varphi$. The diffuse components are represented by straight lines in such a plot. The fraction of the total reflected power contained in the diffuse component clearly increases with decreasing wavelength; the actual percentages are: λ = 68 cm, 17%; λ = 23 cm, 23%; λ = 3.6 cm, 37%; λ = 0.86 cm, 85%. The $\cos^{3/2} \varphi$ dependence of the power at 23- and 68-cm wavelengths is undoubtedly real, but no convincing explanation for such a law has yet been offered. Evans and Pettengill (1963c) supposed that it might represent a combination of Lommel-Seeliger and Lambert scattering – that is, the combined effect of shadowing and the presence of structure comparable with the wavelength. Evans and Pettengill (1963c) demonstrated that a law of the form $\exp-(\text{constant} \sin \varphi)$ provides a poor fit to the quasi-specular component at short pulse lengths, and proposed instead the empirical formula

$$\overline{P}(\varphi) \propto \frac{1}{1 + b\varphi^2} \tag{34}$$

where b is a constant. However, a more careful recomputation of the power in the quasi-specular component shown for λ = 3.6 and 68 cm in Fig. 24 indicates that this law also is a poor fit. A good fit to the experimental results can be obtained from a theoretical treatment of the scattering from a rough surface as described in Sec. I-F.

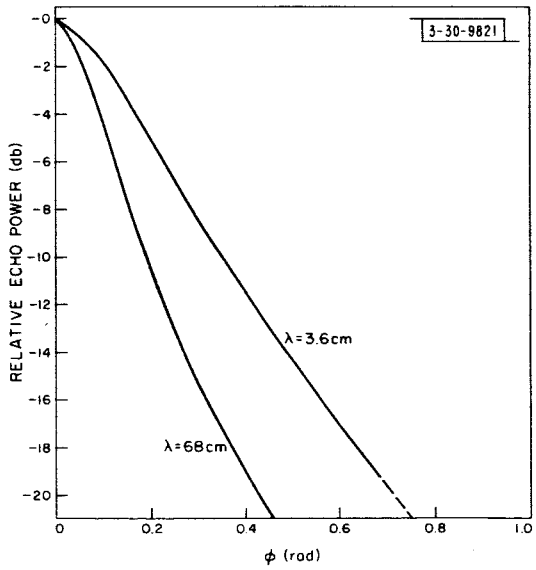

Fig. 24. Quasi-specular component of lunar echoes at 3.6- and 68-cm wavelength. These curves were obtained from results shown in Fig. 23, after subtracting component of power which conforms to straight lines in those plots. Quasi-specular component is believed to be attributable to reflections from large-scale, smooth, undulating parts of surface.

In passing, it should be stated that the separation of the echo power into "quasi specular" and "diffuse" components is thus far warranted only by the fact that the limb regions do appear to scatter according to a law closely resembling the Lommel-Seeliger law. Some support for taking this step comes from the polarization experiments described in the previous section. However, several theoretical attempts to account for the scattering behavior over all φ have been made which do not distinguish between these two regimes. As we shall see from the polarization experiments described in Sec. I-J, such a distinction does seem to be necessary.

F. SCATTERING BEHAVIOR OF IRREGULAR SURFACE

We have seen from the results presented in the previous section that the way in which the moon scatters radio waves is distinctly different from the manner in which it reflects light. For wavelengths of one meter or longer, the moon appears to be a very limb-dark reflector, whereas optically it is almost uniformly bright (Markov, 1948). One may conclude, therefore, that on a scale of one meter the moon is much smoother than on a scale of a few microns. The extent to which it is possible to deduce the statistical properties of the structure on the lunar surface from these results will be reviewed briefly here.

The simplest type of theory is one involving geometric (or ray) optics and has been adopted by a number of authors (Brown, 1960; Muhleman, 1964; Rea, et al., 1964). This has the virtue of avoiding a difficulty encountered in the other treatments: the reflection coefficient will be a function of the angle of incidence and reflection. This difficulty has caused several authors to treat the moon as an irregular perfectly conducting sphere – which is clearly not the case. In the geometric optics approach, only surfaces normal to the line of sight backscatter favorably, and their reflection coefficient is simply the Fresnel reflection coefficient for normal incidence ρ_o. Rea, et al. (1964) show that the amount of power scattered back per unit of the mean surface area per unit solid angle is given by

$$\overline{P}(\varphi) = \rho_o \frac{f(\varphi)}{8\pi \cos\varphi} \tag{35}$$

where $[f(\varphi)/2\pi] \cdot d\Omega$ is the probability that the surface normal lies within a solid angle element $d\Omega$ and makes an angle φ with the normal to the mean surface. It follows that the distribution of surface slopes $f(\varphi)\, d\varphi$ and the mean slope $\bar{\varphi}$ can be obtained directly from the radar measurements of the angular power spectrum $\overline{P}(\varphi)$ (Sec. I-G). One would expect a law of the form of Eq. (35) to describe only the scattering from the large smooth elements of the surface which give rise to the quasi-specular component of the echo (Fig. 24). This follows because a geometric optics treatment is applicable only to the extent that the surface can be regarded as gently undulating, and makes no allowance for small scale structure (which would cause diffraction) and shadowing effects. It is clear from the wavelength dependence of the scattering (Sec. I-E) that the moon's surface does have a considerable amount of structure with dimensions comparable to the wavelength, and it follows that this must become increasingly important as $\varphi \to 90°$.

Other workers have chosen to treat the surface as being perfectly conducting, smooth and undulating and causing no shadowing. The requirement that the surface be smooth is intended

to mean that it contain no structural components having horizontal and vertical dimensions comparable with the wavelength, since the boundary conditions are established locally by means of Fresnel's reflection formulas. It is next commonly assumed (Hargreaves, 1959; Daniels, 1961; Hagfors, 1961; and Winter, 1962) that the probability that the true surface will depart from the mean by an amount h is proportional to $\exp[-\frac{1}{2}(h/h_o)^2]$ where h_o is the rms height variation. Other forms of height distribution (Bramley, 1962) have been used but the theory should not be very sensitive to this function provided that $h_o \gg \lambda$ (Hargreaves, 1959; Daniels, 1961, 1962). This follows because the phase variation in the reflected wave front will be many times 2π radians when $h_o \gg \lambda$ and it becomes impossible to determine h_o from the observations. Once the vertical behavior of the surface is described, it remains only to describe its horizontal structure. This is done by means of an autocorrelation function $\rho(d)$ where

$$\rho(d) = \frac{\overline{h(x)\, h(x+d)}}{h_o^2} \tag{36}$$

in which h(x) is the height of the surface at a point x and h(x + d) at a distance d away. The case where $\rho(d)$ is another Gaussian function

$$\rho(d) \propto \exp\left[-\frac{1}{2}\left(\frac{d}{d_o}\right)^2\right] \tag{37}$$

in which d_o is the horizontal scale size, has been treated by Hargreaves (1959) and Hagfors (1961). If the surface be considered plane and extending in one direction only, then each point on the surface introduces a phase change in the reflected wave of $(4\pi h/\lambda)\cos\varphi$ radian. These phase fluctuations are said to be shallow if the rms phase fluctuation $\Omega = (4\pi h_o/\lambda)\cos\varphi$ is less than 1 radian, and in this case the autocorrelation function describing the variation of radio phase with distance d over the surface will be the same as $\rho(d)$. If, on the other hand, $h_o \gg \lambda$, the rms phase fluctuation Ω becomes greater than 1 radian and the correlation distance in the reflected phase front will fall from d_o to d_o/Ω (since 0, 2π, 4π, ... radians are indistinguishable). At a large distance from the surface, the initial phase variations become modified because overlapping rays and amplitude fluctuations appear. An rms phase fluctuation $\Omega/\sqrt{2}$ is then observed (Bowhill, 1957).

The angular power spectrum $\sigma(\varphi)$ is given by the Fourier transform of the autocorrelation function describing the reflected phase front immediately after reflection, and can be written

$$\sigma(\varphi) \propto \exp[-\frac{1}{2}(\varphi/\varphi_o)^2] \tag{38}$$

where $\varphi_o = \lambda/2\pi d_o$ for $h_o \ll \lambda$ and $\varphi_o = h_o/d_o$ when $\lambda \ll h_o$. It follows that where the wavelength is much larger than the vertical extent of the height fluctuations, the value of φ_o yields directly the horizontal scale of the structure. When $\Omega \geqslant 1$ radian, the determination of φ_o yields the ratio h_o/d_o, that is, the mean surface gradient. This means that for meter wavelength observations of the moon, only the rms surface slope can be determined, and not the actual horizontal or vertical scale sizes. If observations could be made as the wavelength was increased, eventually (when $\lambda > h_o$) it would be possible to determine d_o. However, for the moon this would require low-frequency radio waves which could not propagate through the earth's ionosphere. Daniels (1961, 1962) has discussed at length this limitation in radar observations and has shown that one cannot

obtain information on the rms height fluctuation when this is many times the wavelength in size. It is also clear that small scale height fluctuations $\leq \lambda/8$ will introduce only small phase changes in the reflected phase front and will be unimportant. Thus radar observations may be regarded as being sensitive to structure in the range $\lambda/8$ to about one hundred or so wavelengths. Only by repeating the observations over a wide range of wavelengths can the true nature of the surface be determined.

Forms other than Gaussian have been explored for the autocorrelation function $\rho(d)$. These include exponential

$$\rho(d) \propto \exp(-d/d') \tag{39}$$

(Daniels, 1961; Hayre and Moore, 1961; Hughes 1962a,b) which closely approximates many terrestrial surfaces. Fung and Moore (1964) and Beckmann (1965) have employed a sum of such terms.

When allowance is made for the curvature of the moon's surface, and the physically most plausible series of approximations for the terms in the expression for the reflected field (Huygen's integral) are made, the following results are obtained (Hagfors, 1964).

Gaussian $$\rho(d) \propto \exp\left[-\frac{1}{2}\left(\frac{d}{d_o}\right)^2\right] \tag{37}$$

$$\sigma(\varphi) \propto \frac{\exp[-\varphi^2/2\varphi_o^2]}{\cos^4\varphi} \tag{40}$$

where $\varphi_o = h_o/d_o$

Exponential $$\rho(d) \propto \exp(-d/d') \tag{39}$$

$$\sigma(\varphi) \propto \left\{\frac{1}{\cos^4\varphi + C\sin^2\varphi}\right\}^{3/2} \tag{41}$$

where $C = [d'\lambda/4\pi h_o^2]^2$. Hagfors (1965) has shown that if the statistics of the surface slopes are made the same, the geometric optics approach outlined earlier can be made to yield precisely these same results. Hence, the two approaches are equivalent. If one re-expresses Eq. (41) for small φ, a simpler expression can be obtained,

$$\sigma(\varphi) \propto \left\{\frac{1}{1 + (C-2)\varphi^2 - \frac{C-5}{3}\varphi^4}\right\}^{3/2} . \tag{42}$$

The experimental results for the quasi-specular component observed at 68-cm wavelength are compared with the closest fitting curves corresponding to the laws expressed in Eq. (40) and Eq. (42) in Fig. 25. The exponential result (Eq. 42) provides a much better fit to the measurements than the Gaussian model for the surface autocorrelation function. Similar agreement can be observed for the results at 23- and 3.6-cm wavelengths when the constant C is adjusted to 95 and 36, respectively.

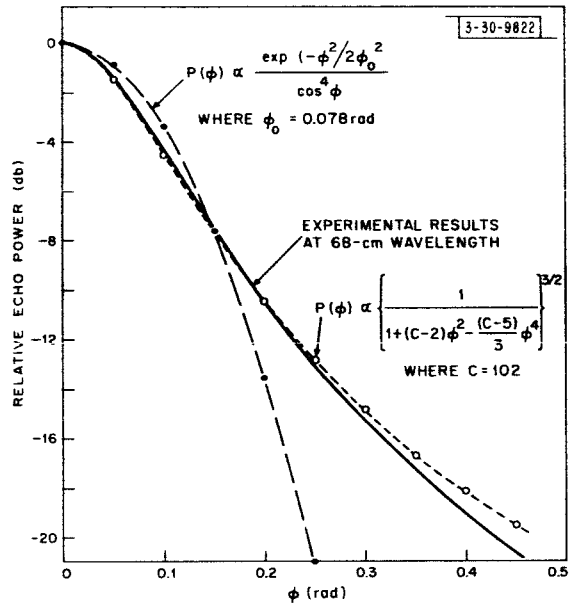

Fig. 25. Values obtained for echo intensity at 68 cm using 12-μsec pulses (after $\cos\phi$ and $\cos^{3/2}\phi$ components shown in Fig. 23 have been removed) compared with the theoretical laws for angular dependence of reflected power.

In the exponential model, the constant C (Eq. 42) contains the wavelength λ. Thus we would expect C to vary as λ^2, yet this does not appear to occur. We must conclude that though the model employing the exponential autocorrelation function (Eq. 39) to describe surface roughness appears to provide a better fit at both wavelengths, it is not characterized by the same value of d'. Presumably the change in wavelength makes the reflection properties of the surface dependent on a different range of structure sizes.

Some authors (Muhleman, 1964; Fung and Moore, 1964; and Beckmann, 1965) have not distinguished between the diffuse and quasi-specular scattering, and have attempted to fit their theoretical results to the whole curve for $\overline{P}(\varphi)$. In some cases (e.g., Beckmann, 1965), they have been surprisingly successful and have argued that this demonstrates that the distinction between the two regimes is artificial. Unfortunately, each author has commenced by assuming that the surface is locally smooth and no theory has properly attempted to account for the presence of small scale structure which must introduce diffraction effects. That such structure must exist can be demonstrated from the wavelength dependence in the scattering behavior. Thus it seems a doubtful procedure to conclude that the theory is adequate, simply because it can be made to match the results by empirically adjusting two or more constants.

At the present time, experimental approaches are being employed in some laboratories to gain a better knowledge of the relation between the statistical properties of a surface and its scattering behavior. In this work, a surface is modeled (usually in sand) over a large area of floor space and the scattering properties explored at millimeter wavelengths.

On a somewhat larger scale, observations of the scattering behavior of the earth's surface conducted with airborne radar equipment can assist in interpreting the lunar echoes. We note that these airborne studies indicate that marked "quasi specular" behavior is encountered only over deserts or the ocean (Grant and Yaplee, 1957; Edison, et al., 1959). Comparisons of the scattering coefficient for the lunar surface and terrestrial terrain have been made, among others, by Safran (1964).

TABLE IV

VALUES FOR RMS OR AVERAGE SLOPE OF UNDULATING PART OF LUNAR SURFACE DERIVED BY DIFFERENT AUTHORS FROM RADAR REFLECTION MEASUREMENTS IN WAVELENGTH RANGE 3 m TO 10 cm

Author	Meter Wave Values for the Average Slope (deg)	Wavelength (cm)	Comments
Hargreaves (1959)	6	250	Rms value obtained by "Gaussian" fit to data published by Evans (1957)
Hagfors (1961)	4	300	Rms value obtained by "Gaussian" fit to the data published by Evans, et al. (1959)
	3	68	Rms value obtained by "Gaussian" fit to the data published by Hey and Hughes (1959)
Daniels (1961)	8-12	68	Average value obtained by "exponential" fit to data published by Pettengill (1960)
Daniels (1963a)	14	70	Average value obtained by "exponential" fit to data privately communicated by J. V. Evans
Daniels (1963b)	6.5	70	Average value after correcting results of Daniels (1963a) for the diffuse component
Hey and Hughes (1959)	3	10	Rms value obtained by "Gaussian" fit to own data
Evans and Pettengill (1963c)	4.5	68	Rms value obtained by "Gaussian" fit to own data
	5	68	Average value obtained by "exponential" fit to own data
Muhleman (1964)	8	68	Rms value obtained by "Gaussian" fit to results of Pettengill (1960). Includes diffuse component
	7	68	Average value obtained by "exponential" fit to results of Pettengill (1960)
Rea, et al. (1964)	11	68	Average value obtained for results of Evans and Pettengill (1963c) when diffuse power subtracted*
	15	68	Rms value obtained for results of Evans and Pettengill (1963c) when diffuse power subtracted*

* Here the slope has been defined somethat differently – see the text.

G. SURFACE SLOPES

From the 68-cm results presented in Sec. I-E different workers have derived values for the average surface slope in the range 5° and 15°. In part, this wide scatter of values reflects differing interpretations of the results. For example, Muhleman (1964) has averaged over the whole $\overline{P}(\varphi)$ curve, whereas Evans and Pettengill (1963c), Rea et al. (1964), and Daniels (1963b) have attempted to subtract the diffuse component of the echo power before computing the slope. Differences also have arisen because most authors weight the values for the slope by the amount of area projected onto the mean surface associated with that slope; yet others, e.g., Rea, et al. (1964), weight by the actual amount of area at each slope. The first method is, in effect, a value for the slope that would be deduced by repeatedly dropping down onto the moon, and the second after walking over the surface and measuring the slopes.

Table IV lists some of the values for the rms or average slope of the lunar surface that have appeared in the literature. They refer to measurements made in the wavelength range 3 m to 10 cm, and hence are roughly comparable. It seems that with the possible exception of the results published by Rea, et al. (1964), none of the values in Table IV are close to the value that would be encountered by a landing vehicle. This follows because most authors have computed the average of the slopes observed when passing a vertical plane through the surface. However, the slope measured in any plane cut through the surface is not necessarily the steepest gradient for that facet, and to obtain the true mean slope encountered by a landing vehicle, one must pass the vertical plane through the surface at all possible azimuth angles. That is, the most meaningful value for $\overline{\varphi}$ is given in

$$\overline{\varphi} = \frac{\int_{\varphi} \varphi f(\varphi) \sin\varphi \, d\varphi}{\int_{\varphi} f(\varphi) \sin\varphi \, d\varphi} = \frac{\int_{\varphi} \varphi \overline{P}(\varphi) \cos\varphi \sin\varphi \, d\varphi}{\int_{\varphi} \overline{P}(\varphi) \cos\varphi \sin\varphi \, d\varphi} \quad . \tag{44}$$

As stated earlier, it is our view that the function $\overline{P}(\varphi)$ employed in Eq. (35) should not be the whole curve but one corrected for the presence of the diffuse component (e.g., the curves shown in Fig. 24). The mean slope obtained by studying all possible planes will be $\sqrt{\pi/2}$ greater than that obtained for a single plane. The rms slope (for a Gaussian surface) will be $\sqrt{2}$ times the rms slope found in a single plane. Hence the values in Table IV [with the exception of those of Rea, et al. (1964)] should be increased by these amounts (Hagfors, 1965).

Essentially the same difficulty in defining what is meant by the mean slope has arisen when an autocorrelation function has been used to describe the surface. Thus, in the Gaussian case, the ratio h_o/d_o is the rms slope only when the distribution is examined in a single vertical plane, and when all such planes are averaged, the rms slope is found to be $\sqrt{2}\, h_o/do$ (Hagfors, 1965). For the exponential autocorrelation function, the relation between the constant C which appears in Eq. (41) and the mean slope has been shown by Hagfors (1965) to be

$$\overline{\tan\varphi} \approx \frac{1}{2\sqrt{C}} \cdot \frac{C-4}{C-\sqrt{C-2}} \cdot \log_e 4C \quad . \tag{45}$$

Equation (45) holds only for large values of C (>100) and Hagfors (1965) concurs with the view of Rea, et al. (1964) that to characterize the slopes by a single number is almost certainly misleading. The most meaningful statement is a curve of $\overline{P}(\varphi) \cos\varphi$ which may be taken as the

probability distribution encountered in a single plane. The results for $\overline{P}(\varphi)$ shown in Fig. 24 have been employed in Eq. (44) to yield values for the mean slope $\overline{\varphi}$ by numerical integration. The results are $\overline{\varphi} = 10.2°$ at $\lambda = 68$ cm and $\overline{\varphi} = 14.8°$ at $\lambda = 3.6$ cm. These values are probably overestimates, since the behavior of $\overline{P}(\varphi)$ for $\varphi < 3°$ has not been properly explored owing to the finite width of the pulse. The mean slope is evidently a function of wavelength, and this reflects the fact that each wavelength acts as a filter and is sensitive only to a given range of structure sizes. It seems probable that the slope obtained by the procedure outlined here will be determined principally by elements of the surface of the order of 10λ across. Thus the average slope observed at 68 cm (10.2°) seems the appropriate value to employ, e.g., for the design of a lunar landing craft.

H. RADAR MAPPING

Provided the radar transmitter and receiver frequencies are determined by very stable oscillators (preferably the same one), it becomes possible to derive spectral information from the phase of the signal. This is achieved by replacing the video detector by two phase detectors driven in phase quadrature by a signal at the same frequency as the center frequency of the echo. The outputs of these two detectors are the sine and cosine components of the signal.

For CW radar observations, the amplitude of the sine and cosine components of the signal can be determined at intervals by means of two sampling voltmeters. The sampling may be thought of as resembling the lines ruled on a spectrum grating. The longer the train of samples (number of lines), the greater will be the resolution obtained. Thus, if samples are taken over a period of 10 sec, a spectral resolution of 1/10 Hz can be achieved. The spacing of the samples ($1/f_s$) determines the spacing of the "orders" in the spectrum. Thus, if no orders are to overlap, it is required that $f_s \geq f_{max}$ where f_{max} is the frequency difference between the lowest and highest frequency components in the signal.

Phase coherent observations of CW moon echoes at 38.25 MHz were attempted by Evans and Ingalls (1962), but unfortunately ionospheric scintillations prevented successful measurements.

For pulse observations, it becomes possible to obtain range and frequency resolution simultaneously by phase coherent observations. At the present time, the technique has been exploited principally by Pettengill (1960), Pettengill and Henry (1962b), and Thompson (1965). When pulse observations are made, the sample frequency f_s automatically becomes the same as the pulse repetition frequency (prf). Thus the prf must be made higher than the spectral width of the signals. As the radar wave frequency is increased, this eventually will lead to a situation where the interpulse period T becomes shorter than the radar depth of the target.

For the moon, the interpulse period T must be greater than 11.6 msec. The Doppler width of the spectrum for a wave frequency of 100 MHz is rarely larger than 2 Hz so that no difficulty should be encountered at frequencies of less than 5000 MHz provided that the gross Doppler shift is properly compensated.

Pettengill and Henry (1962b) made observations at $\lambda = 68$ cm in which a frequency resolution of 1/10 Hz was achieved. Figure 26 shows the power spectrum obtained in this work for the entire moon. It will be observed that both halves of the spectrum are obtained independently. If the rotation period of the moon were unknown, it could be determined from observations such

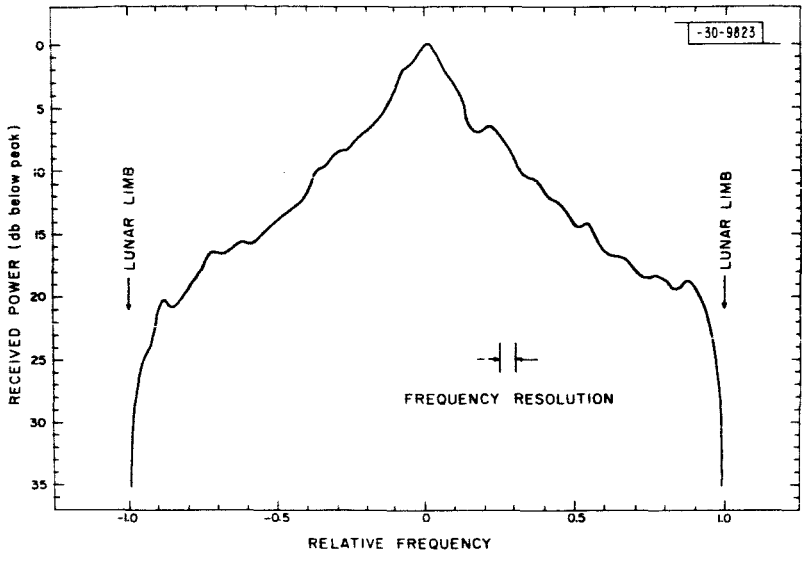

Fig. 26. Power spectrum P(f) of moon echoes obtained by Fourier-analyzing a chain of coherent pulses by means of fast digital computer. These observations were made at 68-cm wavelength and clearly indicate position of limbs.

as these by measuring the Doppler shift of the echoes returned from the limbs. In the case of the moon, the apparent rotation rate is of course well known. If the two halves of Fig. 26 are averaged, the resulting spectrum may be compared with those derived from autocorrelation measurements (Fig. 12). This comparison is provided in Fig. 27, and it can be seen that there is good agreement between both techniques. Figure 28 shows four power spectra for lunar echoes obtained by Pettengill and Henry (1962b) using the Millstone Hill radar at a wavelength of 68 cm. The pulse length employed was 0.5 msec and spectra were obtained for each 0.5 msec of range delay t. Unfortunately for most parts of the disk, there is a twofold ambiguity in the relation between given range and Doppler coordinates and the corresponding surface elements. Also, the contours of constant range and constant frequency become parallel near the limb, causing more surface area to lie in each cell in these regions. Thus the spectra shown in Fig. 28 exhibit what appears to be limb brightening at their edges, which is simply a geometrical effect and is unrelated to the scattering properties of the surface. These spectra exhibited a strong echo in both the polarized and depolarized signals at a range of about 2.85 msec (Fig. 28) which had an intensity of about 7 to 8 times the mean at that range. Pettengill and Henry (1962b) were able to resolve the ambiguity in the position of this scatterer by observing its change in Doppler frequency with respect to the center with time (as a consequence of the projection of the moon's axis of libration changing with time). The discrete scatterer proved to be the crater Tycho.

In many respects, Tycho is well placed for observations such as these. It is at a range where the "quasi specular" component contributes little to the echo, and is not near the edge of the spectrum where the resolution becomes poor owing to the increased area in each cell. If Tycho were nearer the center of the moon, it is doubtful if the range resolution afforded by 0.5-msec pulses would have been adequate to resolve it. These considerations partly explain why only Tycho was identified as an anomalous scatterer in this early work.

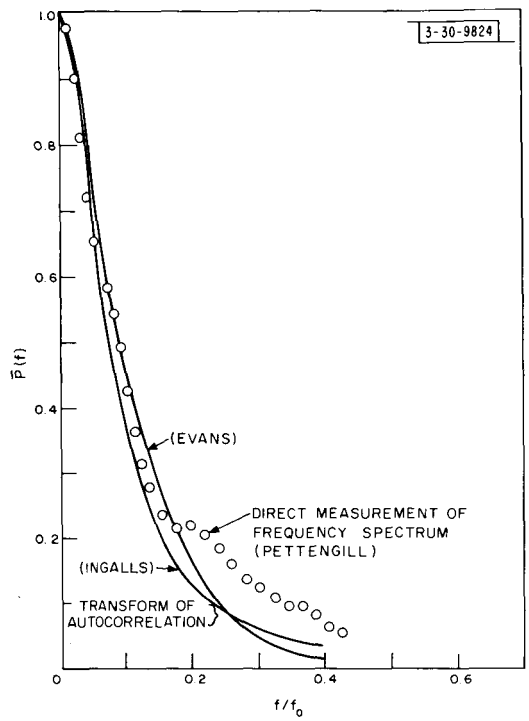

Fig. 27. Power spectrum $\bar{P}(f)$ obtained by averaging two halves of power spectrum in Fig. 26. Also plotted are two power spectra obtained by echo amplitude autocorrelation methods and shown in Fig. 12. It can be seen that all three curves are in reasonable agreement, indicating equivalence of the two techniques.

Shorthill, et al. (1962) have observed that virtually all the rayed craters have anomalous thermal properties at infrared. During eclipses or the waning cycle of the moon, they cool less rapidly than their surroundings. The reverse is true during the waxing phase. Even more spectacular differential cooling is observed during an eclipse (Saari and Shorthill, 1965). This behavior can be attributed to the absence in these recent craters of an appreciable dust layer which overlies most of the remainder of the surface. The extent to which this effect is observed seems to bear a direct relation with the estimated age of the craters concerned (Tycho is the most conspicuous example). It is tempting to suppose that these same craters are also anomalous radar reflectors. Work presently underway to test this hypothesis, at the Arecibo Ionospheric Observatory, has shown that most of the rayed craters are indeed anomalously bright scatterers. In this work, unambiguous maps of regions of the lunar surface are obtained by using an antenna beam sufficiently narrow to discriminate against one of the pair of cells having the same range and Doppler coordinates. Figures 29 and 30 illustrate the level of results obtained by Thompson (1965) during 1964 at the Arecibo Ionospheric Observatory, and show the enhanced scattering observed in the vicinity of the craters Tycho and Langrenus. The superior resolution obtained in these maps over the earlier ones shows that the highest power densities observed in the center of Tycho are nearly ten times stronger than the mean of the surrounding areas. As an older crater, Langrenus appears to exhibit considerably less enhancement. In both figures, the scattering is greatest along the inside crater wall farthest from the radar and the outside rim nearest the radar. This is probably caused by the fact that the inside wall is steeper and is therefore more nearly normal to the ray path than the nearer rim.

The enhancement of the reflectivity of the crater Tycho with respect to its surroundings (by as much as a factor of ten) is of extreme interest, since visually there is nothing obvious that

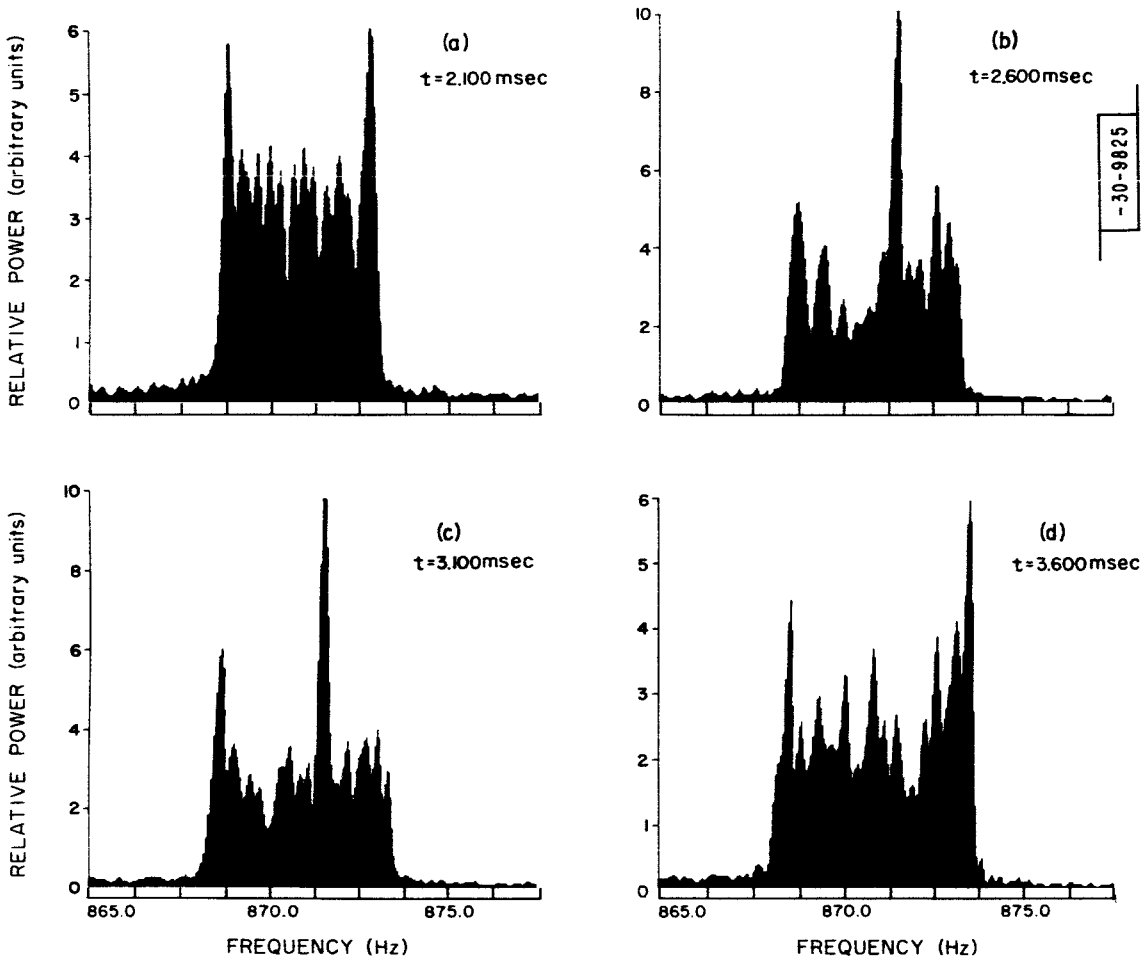

Fig. 28(a-d). Lunar echo power spectra at 4 intervals of range, taken 19h00m19s UT, 20 June 1961. Central peaks in (b) and (c) correspond to position of crater Tycho. Peaks at extremes of spectra result from large common area of intersecting range and Doppler contours and probably do not represent individual surface features.

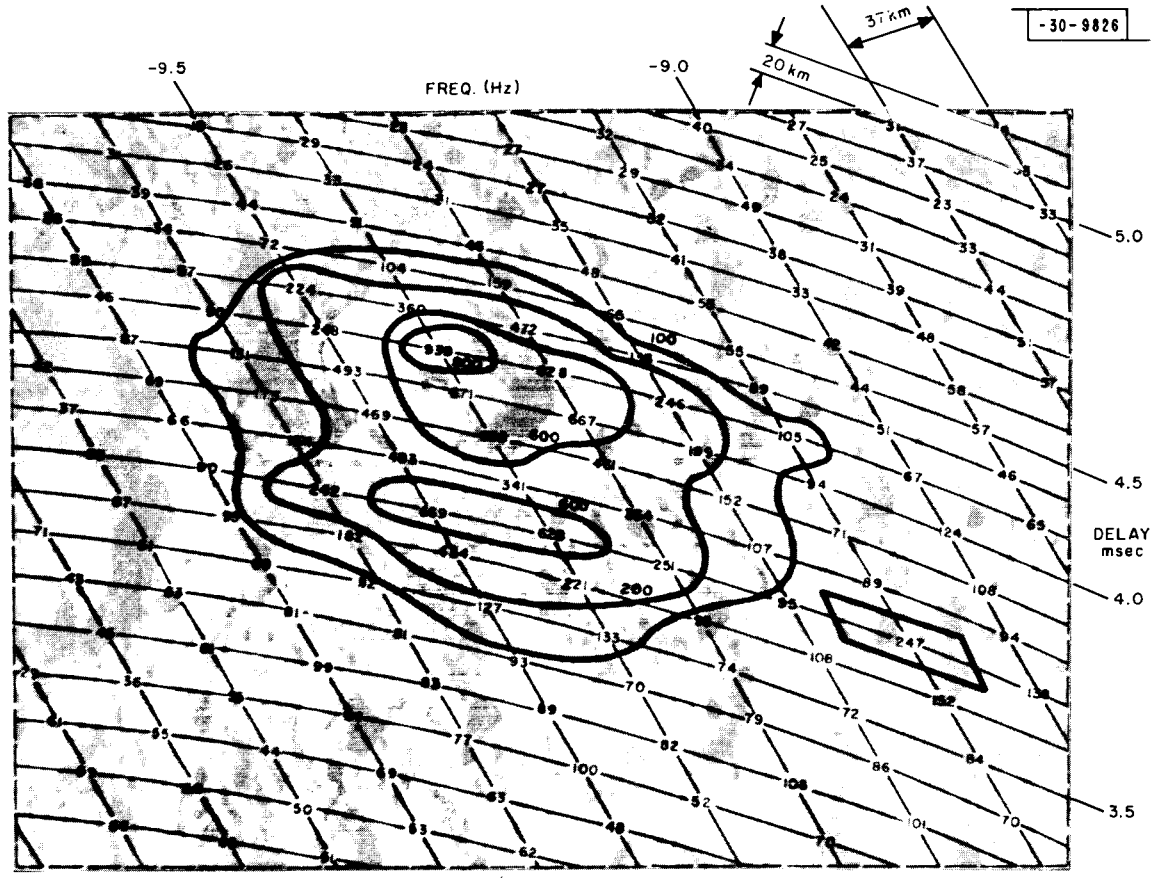

Fig. 29. Results obtained from radar coherent pulse analysis of scattering from vicinity of lunar crater Tycho. In these measurements, radar wavelength of 70 cm and pulse width of 0.1 msec were used. Analyzing resolution was 0.1 msec in delay and 0.1 Hz in frequency. Corresponding geometric resolution on lunar surface is shown in upper right corner. One-hundred individual spectra have been summed for each delay interval. Thus standard deviation of measured power densities (shown above as number proportional to power at intersection of each delay and frequency grid line) is only 10 percent. Power density contours have been drawn for relative levels of 100, 200, 600, and 800. In this experiment, received polarization was set orthogonal to that which would have been returned by specular reflection from properly oriented flat surface.

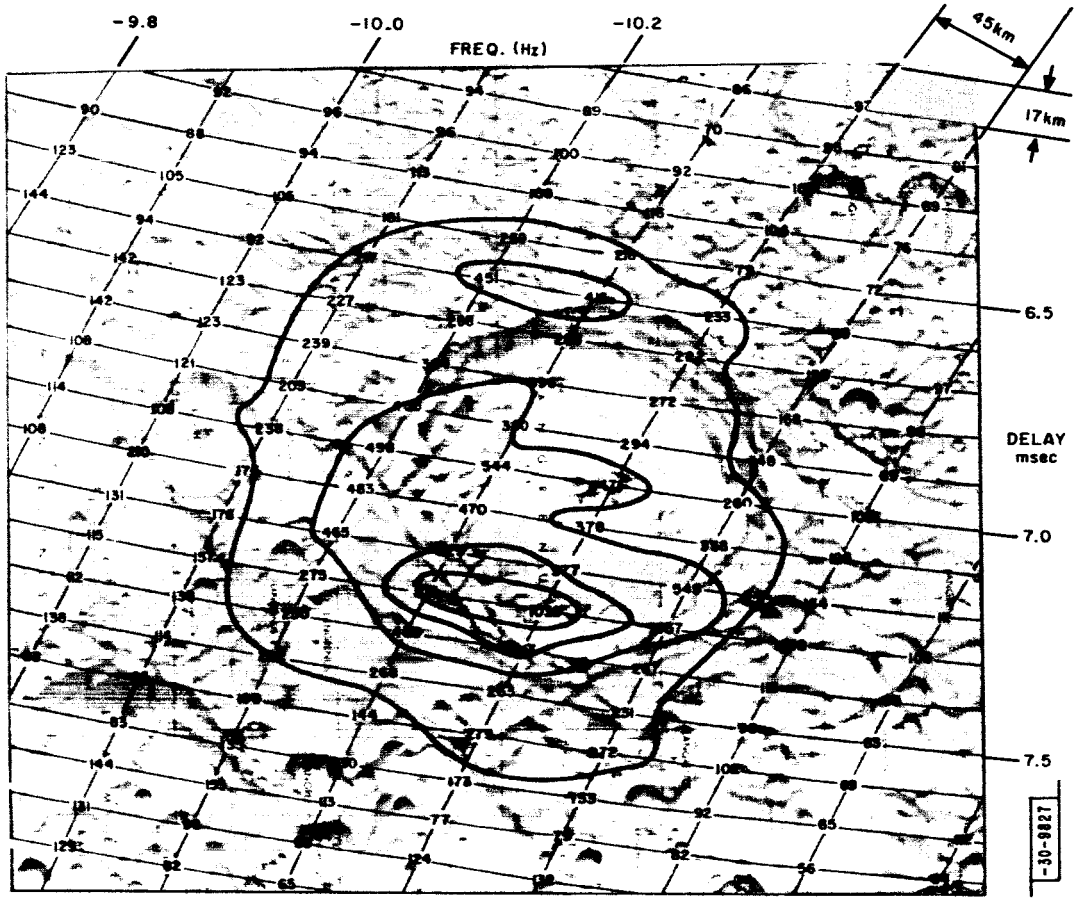

Fig. 30. Radar coherent pulse analysis of scattering from vicinity of lunar crater Langrenus at wavelength of 70 cm. Analyzing characteristics used here are identical to those applied in Fig. 29, except that polarization was aligned to accept specularly reflected energy. Here power density contours represent relative levels of 200, 400, 600, and 800. Note particular enhancement at far wall inside crater and near wall outside rim regions where mean local surface is more favorably inclined to radar beam. Same effect may be noticed in Fig. 29.

distinguishes Tycho from many other craters of comparable size. The fact that it is equally bright with respect to its surroundings for the polarized and depolarized signals precludes any explanation based upon large flat facets normal to the line of sight in the vicinity of Tycho, since these would not be expected to depolarize.

Suppose the surface material in the vicinity of Tycho were solid rock, exposed, perhaps, because there has not been sufficient time since crater formation for the slow but steady environmental processes to have modified it to substantial depths (as they have for most parts of the lunar surface). Then part of the observed enhancement can be explained by the increased reflection coefficient. Some evidence in support of this hypothesis will be presented in Sec. I-J. It also seems reasonable to believe that the extreme roughness associated with fracturing (brecciation) caused by the original meteoric impact is still preserved and visible to the radar. (A thin layer of material overlying the rock could account for the photometric behavior without influencing the radar scattering.) Thus the enhanced reflectivity may be explained as a combination of denser and rougher material in and around the crater as compared with the older unperturbed surroundings.

With the exception of the bright rayed craters, radar maps of the lunar surface seem to be rather featureless. Smaller variations in reflected power have been observed at Arecibo by employing only the resolution afforded by the antenna beam (10 min arc) (Pettengill, unpublished results). From these observations, it was established that the highlands are about 50 percent more reflective than the mare. The reason for this difference is not immediately apparent, though it is tempting to assume that the highlands are rougher than the mare. In all probability the explanation may lie in a combination of increased roughness and density, as is believed to be the case for the rayed craters.

J. POLARIZATION OBSERVATIONS*

In Sec. I-E-3, we described one experiment in which the ability of the surface to backscatter a wave polarized in a mode that would not be encountered for a perfectly smooth specular reflector was examined. The effect of the target on polarizing the exploring wave can be completely specified only after examining the scattering behavior for several different incident and reflected polarizations. For a circularly symmetric body like the moon, these reduce to the experiment described in Sec. I-E-3 and experiments in which linearly polarized waves are incident in three directions on the surface (two at right angles and one along their bisector). Theoretical work by Hagfors (1964) shows that near normal incidence a smooth undulating surface is expected to cause very little depolarization. However, this may not be true for the diffuse scattering regions which are illuminated at large angles of incidence, and presumably cannot be described as smooth.

Combined coherent pulse and polarization experiments have recently been undertaken by Hagfors, et al. (1965), who were struck by the extreme smoothness of the lunar surface as observed in the Ranger photographs (Heacock, et al., 1965). Although a gently undulating and largely smooth surface has been predicted from the radar observations alone, we have also

* The work reported in this section represents part of the work called for under the contract.

seen that a small fraction of the surface is required to be covered with objects having radii of curvature comparable with the wavelength. Few such objects can be found lying on the regions of surface observed by the three Ranger spacecraft.

Hagfors suggested, therefore, that these objects lie beneath the surface, and hence the diffuse tail of the echo (i.e., for delays $t \geq 3$ msec) arises from reflections that have penetrated an upper surface layer. If this were the case and the layer depth were irregular but everywhere greater than the wavelength, one would expect that the echo intensity would depend upon the angle between the incident electric field and the normal to the surface. That is, the component of the incident electric field that lies in the local plane of incidence will couple into the surface best, and hence will be stronger than any other.

In order to test this hypothesis, observations were made using the 23-cm wavelength Millstone Hill radar. The whole moon was illuminated with a circularly polarized wave. This may be thought of as two orthogonal linearly polarized waves separated along the direction of propagation by one-quarter wavelength. The two orthogonal circularly polarized components obtained on reception were combined in such a way that two orthogonal linear components were recovered. This was accomplished by using two hybrid couplers and two variable length sections of transmission line. The orientation of these two orthogonal linear components could be controlled at will and this was continuously adjusted to align one component with the projection of the moon's libration axis into the plane of the antenna (computed in advance).

We now have a situation in which the radar is tracking the moon (in azimuth and elevation), adjustments are continuously being made to the receiver to compensate for the gross Doppler shift of the echo (to an accuracy of better than 0.1 Hz) and the sampling of the signals is being accomplished in such a manner that the continuously changing position of the echo on the time-base is also compensated. In addition, adjustments are made at short intervals to maintain one of the linear components recovered at the receiver aligned with the libration axis.

Finally a large computer is employed for spectral analysis of the returns. In the experiment conducted at Millstone Hill a separate receiver was employed to amplify each of the two linear components, and feed a synchronous quadrature detector. The two sine and two cosine signals that resulted were sampled simultaneously every 160 μsec. Pulses of 200-μsec length were transmitted. Spectra were obtained by processing over a range of $\pm$18 Hz with a resolution of 2 Hz for both linear components at several delays with respect to the leading edge of the echoes. The two spectra obtained at each delay were normalized to include the same area in order to remove any differences in the receiver gains, or noncircularity of the transmitted wave. This is justified, since the circular symmetry of the illuminated annulus makes it almost certain that the total power reflected at a given delay should be independent of the incident polarization.

The component of the signal aligned with the libration axis (component A) will be polarized in the local plane of incidence at the center of the spectrum (i.e., near zero relative Doppler shift) and the orthogonal one (component B) will be perpendicular to this plane. Thus at the center, we might expect $A > B$, if the hypothesis of an irregular layer deeper than the wavelength is in fact correct. On the other hand, at the wings of the spectrum the reverse should be true, i.e., $B > A$.

This behavior is indeed observed, as may be seen in Fig. 31. The extreme frequencies are marked L and points at 0.707 times this value (which ought to appear equally strong) are

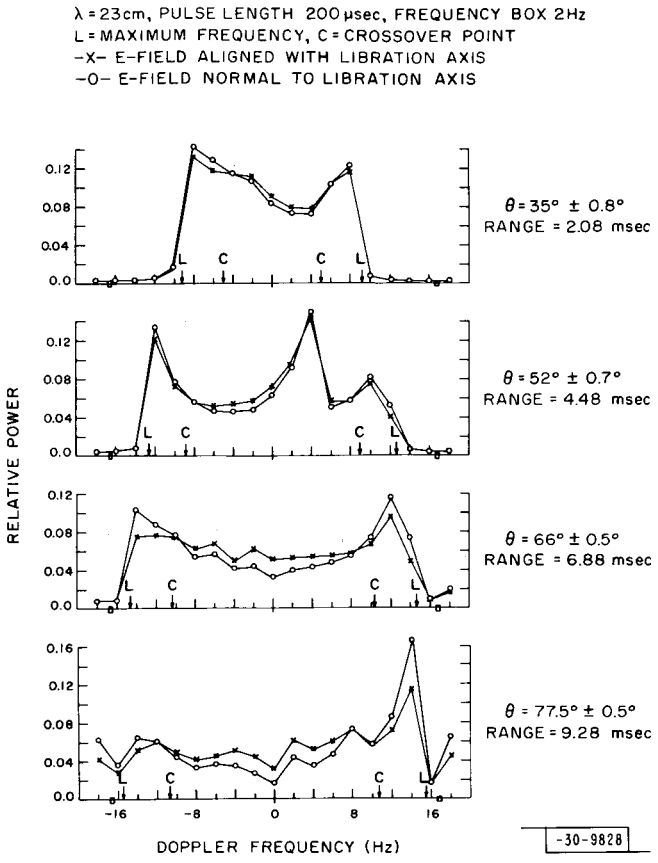

Fig. 31. Spectra obtained at four ranges during course of polarization experiments (18 June 1965, 0340 – 0435 EST) conducted by Hagfors, et al. (1965) which are described in text. Dependence of echo intensity on orientation of incident electric field provides evidence for reflections from within upper layer of lunar surface.

marked C. As can be seen in Fig. 31, the echo curves do cross at the points marked C. A total of 25 minutes' data has been analyzed and included in Fig. 31, so that the statistical uncertainty is only ±2 percent – much less than the systematic effects due to the different polarizations.

One interesting feature in Fig. 31 is the sharp peak at 4.48-msec range plot at a frequency offset of +4 Hz. Here the intensity of the two components is nearly equal, indicating the absence of any layer (compare the ratio at −4 Hz at the same range). At the time of observation, the predicted range-Doppler coordinates of Tycho were 4.30 msec and +2 Hz, and thus it seems plausible to ascribe the anomalous peak to the Tycho region. One might infer that Tycho is not covered by a deep layer of light material, though one much thinner than the wavelength (23 cm) might go undetected. This conclusion supports that reached earlier in Sec. I-H that Tycho must contain large areas of exposed solid rock in order to account for the intensity of the echo.

K. DIELECTRIC CONSTANT

In Sec. I-B we introduced two generalized radar equations for an irregular sphere,

$$\sigma = g\rho_o \pi a^2 \qquad (8)$$

and

$$\sigma = G_m \bar{\rho} \pi a^2 \quad . \tag{10}$$

We have seen from the results of Sec. I-E that the moon appears to scatter in part as a smooth undulating sphere and in part as a collection of small scale, almost isotropic, scatterers. At 68-cm wavelength, the ratio of the powers due to these two parts is 4:1.

In attempting to derive a value for the dielectric constant k, Evans and Pettengill (1963c) supposed that a fraction X of the actual surface area could be associated with the diffuse component, and further that these scatterers obeyed the Lambert law [Eq. (12)] for which the gain $G_m = 8/3$ (Grieg, et al., 1948). The remainder of the surface they took to be smooth and undulating and assumed it to have a directivity factor $g \rightarrow 1.0$. Hagfors (1964) has since shown that $g = 1 + \alpha^2$ for the smooth part of the surface where $\alpha = h_o/d_o$ for a Gaussian surface [Eq. (37)] and hence is related to the rms slope (Sec. I-G). Since $\alpha \sim 0.1$ at $\lambda = 68$ cm, it follows that $g \rightarrow 1.0$ and the assumption $g = 1.0$ made by Evans and Pettengill (1963c) is not a bad one. The total cross section σ was thus obtained as the sum of two parts, the smoother being obtained from Eq. (8) and the rough from Eq. (10), thus

$$\sigma = [(1 - X)\rho_o + \frac{8}{3} X\bar{\rho}] \pi a^2 \quad . \tag{46}$$

With no real justification, Evans and Pettengill (1963c) equated $\bar{\rho}$ to ρ_o, since otherwise Eq. (46) cannot be solved. The error introduced into the value for the dielectric constant k is likely to be small, because the second term in Eq. (46) has a value of only one-quarter of the first. However, the value for X (which is found to be 8 percent) might be somewhat in error. At all events, the cross section was then written

$$\sigma = [(1 - X) + \frac{8}{3} X] \rho_o \pi a^2 = 0.074 \pi a^2 \quad . \tag{47}$$

From this, ρ_o was calculated to be 0.065, and this led, via Eq. (7), to a dielectric constant k = 2.79. Evans and Hagfors (1964) applied these arguments to the observations conducted at 3.6 cm and 8.6 mm to obtain the results shown in Table V.

TABLE V

VALUES FOR REFLECTION COEFFICIENT AT NORMAL INCIDENCE ρ_o AND DIELECTRIC CONSTANT k DEDUCED BY EVANS AND HAGFORS (1964)

λ (cm)	Power In Diffuse Component (percent)	X (percent)	ρ_o	k
68	20	8	0.065	2.79
3.6	30	14	0.060	2.72
0.86	85	68	0.035	2.13

We have remarked that provided the amount of power in the diffuse component remains small, this series of approximations probably does not introduce serious error in the value for k, although the percentage area of the surface X that is rough may be in error. When the largest part of the power appears in the diffuse component (at 0.86 cm), it is doubtful that Eq. (47) has much validity. Hence, little significance should be attached to the apparent wavelength dependence in k shown in Table V. However, it is clear that the roughness does increase with increasing frequency, and the absence of a corresponding increase in the cross section must mean that the reflection coefficient is decreasing. Such a wavelength dependence could result either as a consequence of a finite conductivity s in the medium (Eq. 6), or the surface may be inhomogeneous and have density variations with depth.

A somewhat more rigorous approach to the problem of dealing with the smooth and rough portions of the surface has been published by Rea, et al. (1964). In this approach, the moon is assumed to be covered with equal-sized flat facets having a distribution of slopes $f(\varphi)$. The cross section can then be computed and the directivity g is simply the ratio of the actual area to the projected area ($2\pi \int_0^{\pi/2} f(\varphi) \sin\varphi \, d\varphi$). In order to obtain $f(\varphi)$, Rea, et al. (1964) subtracted from the observed echo power function $\overline{P}(\varphi)$ the power in the orthogonal component $\overline{D}(\varphi)$. In this way they sought to remove the influence of the small scale roughness in determining $f(\varphi)$. Since it is not clear what fraction of the incident energy one might expect to appear in the depolarized component, several possibilities were tried:

$$\begin{aligned}
&\text{Case 1} \quad f(\varphi) \propto \overline{P}(\varphi) \\
&\text{Case 2} \quad f(\varphi) \propto \overline{P}(\varphi) - \overline{D}(\varphi) \\
&\text{Case 3} \quad f(\varphi) \propto \overline{P}(\varphi) - 2\overline{D}(\varphi) \\
&\text{Case 4} \quad f(\varphi) \propto \overline{P}(\varphi) - 3\overline{D}(\varphi)
\end{aligned} \tag{48}$$

If we assume that at the limb only small scale elements contribute to the scattering, then we might expect case 4 to be closest the truth. This follows from the results of Sec. I-E-3 which showed that the ratio of $\overline{P}(\varphi)$ to $\overline{D}(\varphi)$ at the limb is approximately 3:1. Rea, et al. (1964) concluded that the actual case lay between 3 and 4 by a similar process of reasoning. The fraction of the total power remaining for case 4 was found to be 0.85, and the directivity factor g determined by graphical integration was 1.11. By assuming a total cross section $\sigma = 0.074\pi a^2$, the corresponding reflection coefficient ρ_o was found to be 0.057, leading to a dielectric constant $k = 2.6$.

In view of the recent experiments carried out by Hagfors, et al. (1965) and described in the preceding section, it is evident that any value for the dielectric constant derived from the strength of the echo power near normal incidence must represent some composite average, since reflections apparently come from both the top of and within the surface.

In order to test further the hypothesis of a penetration mechanism through a tenuous top layer on the lunar surface, the ratio of the power in the two orthogonal linearly polarized components was computed as a function of the angle of incidence on the mean lunar surface. This information was most readily derived from the spectra shown in Fig. 31 near zero frequency. The same information could, in principle, be derived from the maximum frequency regions also, but in these latter regions the angles between the planes of polarization and the plane of

incidence changes much more rapidly with changes in frequency offset than they do near zero frequency, and for this reason the ratios were computed only on the basis of information derived from the power spectra near zero frequency offset.

It was next assumed that for all the delays examined and plotted in Fig. 31, the echo is wholly the result of reflections from within the surface. This assumption is reasonable in view of the large angles of incidence to which these delays correspond. It seems that it would be extremely unlikely to encounter flat regions of the surface normal to the incident wave. The possibility that small scale structure lies on the surface and contributes to the echo remains. The Ranger pictures (Heacock, et al., 1965) indicate that few elements of the surface have radii of curvature comparable to 23 cm, but this cannot be regarded as an absolute guide.

A second assumption was next made; namely, the scattering mechanism within the surface converts little of the incident power into an orthogonal mode. This too seems reasonable on the basis of the results presented in Sec. I-E-3 which showed that circularly polarized waves are returned in the expected sense more strongly than the depolarized sense even in the diffuse part of the echo.

A third and final assumption was that the reflection process inside the layer is independent of the polarization angle. This will be true if the signals are backscattered from an irregular layer. The relative strength of the two components then depends only upon the square of their respective transmission coefficients (since the wave passes through the boundary twice). In Fig. 32, the square root of the ratios derived from the ratio of the backscattering coefficients is plotted against the mean angle of incidence. The same diagram shows the ratio of the corresponding transmission coefficients for dielectric constants of 1.5 and 2.0. As might be seen, it is very tempting to ascribe a dielectric constant of about 1.7 to 1.8 to the top layer.

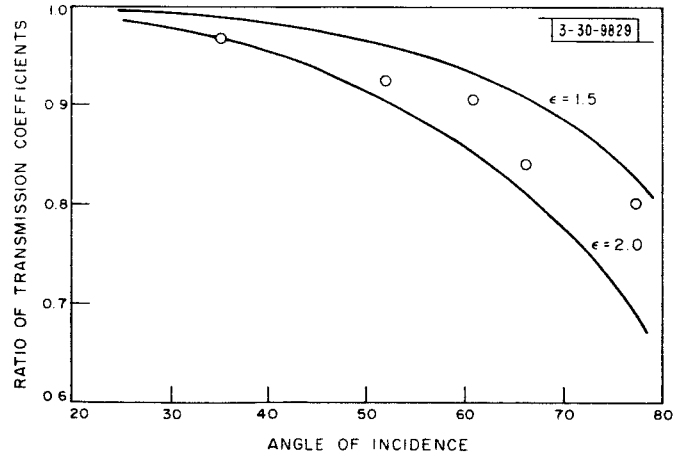

Fig. 32. Ratio of square root of echo powers observed for two linear components whose spectra are plotted in Fig. 31. If all power is scattered from within, surface is at large angles of delay, and further if there is no spill-over from one linear component into the other, then this is ratio of transmission coefficients into surface. Experimental values suggest that upper layer has dielectric constant of 1.7 to 1.8.

It is evident that if at these delays substantial amounts of power are reflected without penetrating the surface, or that if substantial amounts are converted into orthogonal modes, the points in Fig. 32 will be higher than they should be. Similarly, if parts of the surface are not covered by a layer of material, the points will be raised. Thus a value of 1.7 to 1.8 for the dielectric constant of the layer can be taken as a definite lower limit.

Let us suppose, then, that the lunar surface consists of two layers. The upper one is irregular in depth, largely smooth, and has a dielectric constant of 1.8. It is interesting and probably significant that this value corresponds very closely to the ones derived from radiometric observations of the polarization of the thermal emission from the lunar surface (Soboleva, 1962; Heiles and Drake, 1963) and other values inferred from passive observations (Troitsky, 1962; Salomonovich and Losovsky, 1962; Krotikov and Troitsky, 1962). All these values were found to lie in the range 1.5 to 2.0, and hence disagreed with the radar value (2.6 to 2.8) derived earlier in this section.

The radiometric determinations of the dielectric constant based on the polarization of the thermal emission can be brought into line with this naïve two-layer model. Calculations show that near grazing angles of incidence, the polarization of the emission will practically be determined entirely by the top layer. It therefore appears that a two-layer model of the lunar surface of the type suggested provides a rather self-consistent explanation of several different types of observations made of the moon by radio waves. The simple two-layer model suggested could be refined by introducing a gradual change in the dielectric constant with depth, but as yet it does not appear that the experimental data warrant such a refinement.

If a two-layer model of the surface is accepted as a working hypothesis, what are the other properties that can be derived? In order to reconcile the observed reflection coefficient at normal incidence (5.5 percent) with that expected for a homogeneous layer having a dielectric constant $k = 1.8$ (2.1 percent), it is necessary to have a base layer with a dielectric constant $\epsilon = 4.5$ to 5. The base layer is also required to be somewhat rougher in order to give rise to backscattering at large angles of incidence.

As to the depth of the layer, one can say only that it must be irregular and greater than 23 cm (the wavelength employed in these observations). If the depth is less than, say, one or two meters, one would be able to account for the increase in cross section observed by Davis and Rohlfs (1964) (see Table II), since a thin layer would be unimportant at such wavelengths. However, as noted earlier, these long wave measurements are extremely difficult to perform reliably and perhaps not too much importance should be attached to this possible upper limit.

In view of the fact that at normal incidence some 60 percent of the echo power appears to be reflected from within the surface, we are obliged to question the meaning of the distributions and rms values of the surface slopes obtained in Secs. I-F and I-G. These values cannot apply to the uppermost layer, but to some hypothetical surface lying within that layer. For a two-layer model, this hypothetical surface would lie roughly midway between the two boundaries and have characteristics comparable to the sum of the two layers. It follows that since the hypothetical surface is largely smooth and undulating neither boundary can be particularly rough.

In our present interpretation, we have ascribed the small scale roughness entirely to the base layer, but this may be improper. A variety of models can be invented which would match

the results. For example, the base layer could be equally as smooth as the top, and irregularities in the density of the upper layer (e.g., boulders) might be responsible for the diffuse component.

L. PACKING FACTOR OF LUNAR MATERIAL

Some constraints can be placed on the packing factor W_o which describes the fraction of the volume occupied by the surface material. If W_o is small, then it seems that an expression developed by Twersky (1962) which relates the observed dielectric constant k_{obs} to that of the material in bulk should apply. If the surface is assumed to consist of grains of pure dielectric material whose size is small compared with the wavelength, and which are well separated so that they can act as independent dipoles, the observed dielectric constant will be

$$k_{obs} = 1 + \frac{3E}{1 - E} \tag{49}$$

where $E = W_o(k - 1)/(k + 2)$, in which k is the dielectric constant of the material in bulk. Where W_o is large and the surface can more properly be modeled as a continuous dielectric with small, well-separated cavities embedded in it (which now act as the scatterers), then a formula developed by Odelevskii and Levin (see Krotikov and Troitsky, 1962) should apply

$$k_{obs} = k\left[1 - \frac{3(1 - W_o)}{\frac{2k + 1}{k - 1} + (1 - W_o)}\right] . \tag{50}$$

The two formulas can be shown to be equivalent by regarding the holes in the second model as vacuum spheres suspended in a dielectric and using Eq. (49) to recover Eq. (50).

If we assume that the lower layer is largely silicate material, then the value for the dielectric constant that has been derived (ϵ = 4.5 to 5.0) indicates that this material must be more or less solid. If in addition we assume that the upper layer consists of the same material, but broken and more porous, then from Eq. (49) we conclude that W_o = 45 percent and from Eq. (50) W_o = 30 percent.

Since it is not clear which of these values is the better one to take, we have plotted in Fig. 33 the variation of the observed dielectric constant k_{obs} with W_o derived from Eqs. (49) and (50), together with some experimental points reported by Brunschwig, et al. (1960) for sand. It appears from this comparison that Eq. (50) provides a much closer fit to the experimental results. It is evident from Fig. 33 that the value observed for the upper layer, k_{obs} = 1.8, would be consistent with a light sand having a packing factor of 0.3. Since quartz has a rather low value of k (see Table I), this may perhaps be taken as an upper limit to the value of W_o. A lower limit can be obtained by putting k = 20, whence W_o = 0.10 is obtained.

It is, of course, not possible to say anything, on the basis of the radar results, concerning the bearing strength of such a light material. This must depend considerably on the physical structure of the material, and presumably the rock froth envisaged by Kuiper (1965) and others would have a greater strength than the dust layer conceived by Gold (1962).

M. SUMMARY

The results which have been described were obtained principally using radar systems operating at decimeter wavelengths. It appears that at normal incidence, some 60 percent of the

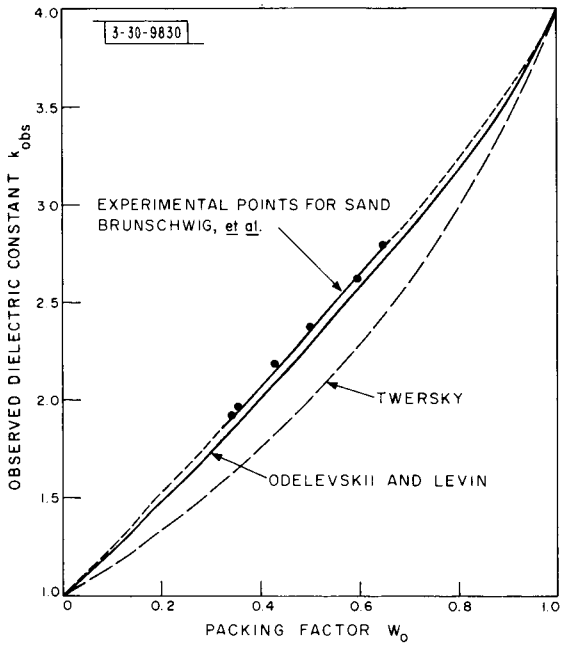

Fig. 33. Variation of observed dielectric constant k_{obs} with packing factor W_o of quartz having bulk value of dielectric constant k = 4. Packing factor W_o is defined as ratio of density of actual broken material to material in bulk. Results obtained from two theoretical formulas [Eqs. (49) and (50)] are here compared with experimental results reported by Brunschwig, et al. (1960) for sand.

echo energy is reflected from within the surface, presumably at points where the density increases rapidly with depth. The uppermost layer of this surface has a dielectric constant of not less than 1.8, which implies that it has a porosity in the range from 70 to 90 percent, depending upon the nature of the material.

If it is assumed that there is only a single reflecting layer within the surface (two-layer model), the dielectric constant of the base layer must be 4.5 to 5.0 and the material there quite compacted if not actually solid. The depth of the upper layer must be greater than about 23 cm, and irregular, but beyond this little more can be said at present.

The two boundaries appear to be characterized by smooth surfaces with rms slopes of the order of 1 in 10. The lower boundary is presumed to be rougher than the upper one. In order to account for the fact that 20 percent of the power lies in the diffuse component at 68-cm wavelength, we require that a comparable fraction of the area of the base layer be covered with structure of the order of the wavelength in size.

A two-layer model of the surface as envisaged here is, in all probability, a mere approximation. It seems likely that the density will increase continuously with depth, since a material with a porosity of 70 to 90 percent could perhaps hardly support its own weight to any considerable depth. If this is the case, the reflection from within the material will be a function of how rapidly the density changes in a depth of one wavelength. Thus the shortest wavelengths may be reflected almost entirely from the uppermost interface, and longer wavelengths will be increasingly reflected from within the material. It seems that by exploiting the technique of range-Doppler mapping with controlled polarization at a number of wavelengths, the properties of this layer can be explored further. At this time, this seems to be the primary ground-based technique for making such studies.

II. RESEARCH HIGHLIGHTS THIS QUARTER

A. EXPERIMENTAL OBSERVATIONS

During this reporting period, lunar operations have utilized the 23-cm wavelength Millstone radar. The 3.8-cm wavelength radar system at the Haystack research facility, though fast progressing, is not observing the moon as yet, while the 8.6-mm wavelength radar is not yet operational. An account of the program of readying these two radar systems for lunar observations will be given in the next quarterly progress report and early Haystack results should be available.

The Millstone radar was used during the reporting period, and somewhat before, in measurements to determine the scattering properties of the moon at 23-cm wavelength using a variety of transmitted and received polarizations. A full report on this work is in preparation and will be reserved for a later quarterly progress report. Some profoundly important results of this work, however, are summarized here.

One of these results is strong evidence for the existence of a layer of light material overlying most of the lunar surface. This material appears to be very porous (70 to 90 percent) and at least 20 cm deep. The material may be supported by a solid layer at some (as yet) unknown depth, or the density may increase gradually from dust, e.g., to sand, thence to rubble and finally to solid rock. It is not possible to distinguish between these possibilities on the basis of present evidence. It is possible that the layer of light material is only of the order of a few tens of centimeters deep, since there is some evidence (albeit rather inconclusive) that at a wavelength of 15 meters the reflection coefficient corresponds to that of the supporting layer alone. The importance of this discovery cannot be overemphasized. It has thus been included in the review of radar studies of the moon given in Sec. I. The experiments leading up to these conclusions are described fully in Sec. I-J.

Previous to the reporting period, the distribution of echo power with delay over the lunar disk (which defines the angular scattering law as shown in Sec. I-E) had been determined over the full radar depth only at a wavelength of 68 cm. The new measurements (presented in Table III and Fig. 19 of Sec. I) yielded similar results at 23-cm wavelength. These support the conclusion reached earlier that the scattering behavior of the lunar disk is markedly wavelength dependent.

The depolarizing properties of the surface have also been explored in this work, using both circularly and linearly polarized signals. These measurements support the conclusions reached in Sec. I-E-3 concerning the presence of a class of scatterer (believed to lie within the surface – Sec. I-J) which can depolarize the incident signals and as such must have radii of curvature comparable with the wavelength.

B. THEORETICAL WORK

In addition to the experimental work outlined above which forms the substance of a later report, theoretical work has been carried out concerning the influence of shadowing on the scattering from a rough surface. At least one previous attempt [Beckman (1965)] to compute the effects of geometrical shadowing (i.e., ignoring diffraction) on the scattering behavior

has been made. In this computation, it was assumed that the shadowed regions were completely removed from view and it was shown that the statistical distribution of surface slopes visible to the radar remained unchanged. Thus, if the function $S(\varphi)$ gives the fraction of the area left visible to the radar for an angle of incidence φ and the angular scattering law in the absence of shadowing is $P(\varphi)$, one would observe a function $f(\varphi) = P(\varphi) \cdot S(\varphi)$.

We have since learned that there is a mathematical mistake in the function $S(\varphi)$ derived by Beckmann. However, even in the absence of any errors we do not believe that the function $P(\varphi) \cdot S(\varphi)$ represents the observed scattering dependence, for the reason that the distribution of slopes visible to the radar will change when the surface is shadowed. What is important is not the amount of area removed from view but the number of elements normal to the ray path that are removed from view. These two are not the same. Intuitively, this may be seen as follows. The surfaces which are most effective in shadowing are those normal to the ray path. These are, however, the most favorable backscatterers. The regions they remove from view are largely the reverse slopes of hills which would not reflect favorably in any case. Thus, even if shadowing function $S(\varphi)$ were not formally wrong, we believe that it would overestimate the effect of shadowing.

To test the validity of this reasoning, the scattering from a rough surface in the presence of shadowing has been modeled in a digital computer, using Monte Carlo methods. The results of this work confirm the above statements and have yielded some quantitative estimates of the geometrical effects of shadowing. A full report on the work will be given in a later technical report.

C. STUDIES FOR FUTURE EXPERIMENTS

Though the experiment which demonstrated the presence of an unconsolidated layer was not capable of yielding an upper limit to the depth of the material, it is conceivable that such an upper limit may be obtained from ground-based radar experiments. Some thought has been given to the matter and it appears that there are at least two possible avenues. By repeating the experiment described in Sec. I-J at longer wavelengths, one might eventually reach a wavelength at which the polarization disappears, indicating that the layer depth is only a fraction of that wavelength. The alternative might be to increase the wavelength and search for an increase in reflectivity which will occur when the layer depth becomes a small part of a wavelength.

Technically, both these experiments are difficult to perform for a variety of reasons. The instrumentation required is not owned by Lincoln Laboratory, although the Arecibo Ionospheric Observatory operated by Cornell University should be well suited to such experiments. The next quarterly progress report will contain a discussion of these ground-based radar methods of arriving at the depth of the material.

The ability to determine the average depth $\bar{D}$ of the layer of dust on the moon from the earth depends largely upon whether it is as deep as the longest wavelength λ that can penetrate the earth's ionosphere without suffering serious scintillation effects. This is of the order of $\lambda = 10$ m, and if $\bar{D}$ is greater than about 2 or 3 m, the two techniques outlined above would run into severe difficulty. It is possible, therefore, that a lunar-orbiting radar may be needed to obtain this information, assuming that $\bar{D} > 5$ m, and that the Surveyor missions encounter further delays or difficulties. We have not yet considered radar experiments that may be performed from spacecraft in any detail, but will endeavor to do so later.

III. REVISED RESEARCH PLANNING

A. BACKGROUND

In the Foreword we mentioned that recent results have indicated the need for a slight change of emphasis in planned measurements. The section therefore reviews the program as now planned, and the time scale in which we hope to carry out the work.

The experiments that were planned for Millstone to measure radar cross-section echo power vs range and polarization studies at 23-cm wavelength with R-$\dot{R}$ mapping will be largely completed early this year. In addition, some radiometric studies at Haystack have now been carried out. Prior to this new work, it was not known whether measurable amounts of radiowave energy were reflected from within the lunar surface. Consequently, it was not known if the polarization studies at 23 cm would show the existence of an angle of incidence dependency from which the dielectric constant of the surface material could be deduced. As we have seen (Secs. I-J and I-K), such effects are indeed observed and provide a direct method of deriving the dielectric constant. We consider that by exploiting this technique as a function of wavelength, we may obtain the depth of the layer of light material on the surface. We now hope to perform polarization experiments at 3.8-cm and 8-mm wavelengths. It is understood that the Arecibo Ionospheric Observatory will carry out similar measurements at 68-cm.

B. PLANNED EXPERIMENTS

The program of work falls into two broad classes:

(1) Experiments which yield information about the average properties of the lunar surface

(2) Experiments which yield information about localized regions.

Figure 34 shows the work now planned to cover (1) and Fig. 35 that planned for (2). None of the experiments indicated in Fig. 35 is new. All have been carried out at least at one wavelength and some at more than one. What is now important is to carry out these measurements at a number of wavelengths and hence derive the dependence upon λ. Herein lies one of the chief virtues of joint studies with the Arecibo Ionospheric Observatory. The radar systems operated by the Lincoln Laboratory and Cornell University span a range λ = 7.5 m to λ = 8.6 mm, or about 100:1.

Two average properties of the lunar surface that may be derived by radar observations are: (1) the electrical constants (e.g., dielectric constant) as a function of depth and (2) the distribution of surface slopes measured over some given spacing. The radar wavelength λ controls the spacing in (2) in a direct fashion, since the derived slopes may be associated with spacings of the order 5 to 10 λ.

The interpretation of the measurements to determine the angular scattering law is open to certain refinements; for example, the effects of diffraction and shadowing have not yet been properly included (Sec. I-F). On the other hand, the derivation of the distribution of the slopes and rms slope from these data is relatively straightforward. The experiments shown in Fig. 35

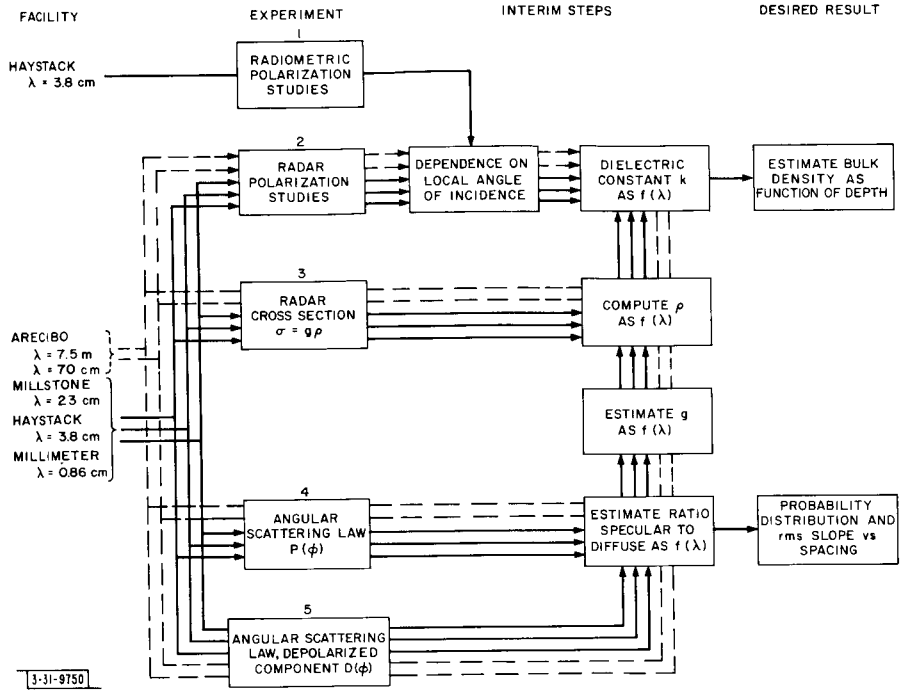

Fig. 34. Experiments to determine average properties of lunar surface.

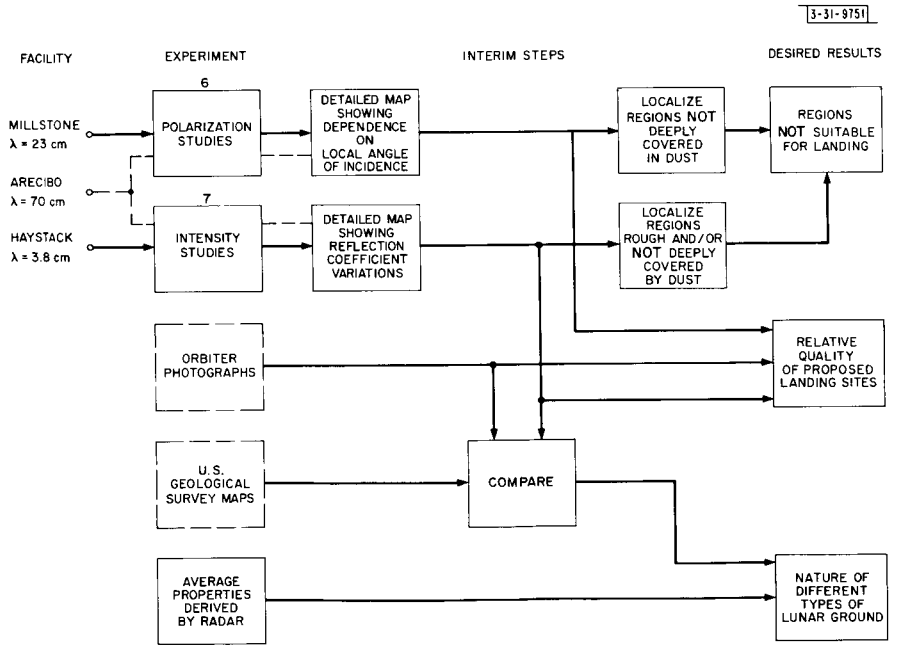

Fig. 35. Experiments to determine properties of local regions on lunar surface.

as Experiment 4 have largely been completed and the results have been reviewed in Secs. I-E and I-G. It is unlikely that the additional measurements will yield a great deal that is new.

The wavelength controls the depth of penetration [important in (1)] in a way which depends upon the electrical conductivity. Unfortunately, the electrical conductivity of the lunar surface is not yet known and hence there is large uncertainty in our knowledge of the depth to which the waves penetrate. Accordingly, measurements of reflection coefficient at a single wavelength are difficult to interpret in terms of a dielectric constant at a given depth. On the other hand, the polarization experiment listed as Experiment 2 yields directly the dielectric constant of the uppermost layer of light material. By repeating this experiment at a number of wavelengths, we may be able to establish the average depth of this layer. In the event that the properties of the surface change with depth gradually and continuously so that there is no discrete boundary within the material, it may, of course, prove a difficult task to deduce the precise character of the surface from radar measurements. However, we presently feel that the best hope lies in examining both the reflection coefficient and polarizing ability as a function of wavelength.

To derive the properties of localized regions of the lunar surface, we plan to use the delay-Doppler technique (Sec. I-H). By repeating the polarization measurements made at Millstone with better resolution, it should be possible to isolate additional regions which, like Tycho, do not appear to be covered with an appreciable layer of light material.

Mapping the reflectivity over the surface leads, as we have seen (Sec. I-H), to the identification of rough and/or dense regions (i.e., regions where solid rock is exposed to the view of the radar). The mapping of the reflectivity can be carried out at Haystack and Arecibo to a resolution of 5×5 km or better. Thus, this work will identify regions that are unsuitable for landing and, in addition, can be employed to gauge the relative quality of proposed landing sites. Other information (e.g., the orbiter photographs) is, of course, expected to contribute to such a comparison.

There is considerable interest in examining the radar maps produced at $\lambda = 3.8$ cm and $\lambda = 70$ cm for similarity. Differences between the two will largely be attributable to the different depths of penetration of the two waves. This comparison, together with separate comparisons with the U. S. Geological Survey, may show that different types of lunar ground can be identified by their radar reflectivity. If this is the case, radar can be employed to extend knowledge gained for a particular area to the rest of the lunar surface, since potentially it is a fast method of surveying.

The work indicated in Fig. 35, while straightforward in concept, will in fact consume the largest amount of time and effort in the whole program. It is expected that the central portions ($\pm 10°$ of selenographic latitude) of the lunar surface (i.e., including the proposed landing sites and photographic orbiter sites) will have been mapped by the date of completion of the contract; it is unlikely that substantially more than this can be accomplished in that time period.

C. INSTRUMENTATION NOTES

The 23-cm work depends upon the Millstone L-band tracking radar, which is a proven facility. The completion of the work at this frequency is being speeded, however, by the new computing facility accepted during 1965. Five equipment highlights are listed here, some of which were started prior to the present contract:

(1) Direct interfacing of this machine to the radar system has progressed well.

(2) Intersite coupling arrangements have been completed, permitting the signal-processing complex at Millstone to operate with the Haystack X-band radar system.

(3) A special-purpose processor has been specified for use with this computer which will greatly speed the specialized computations in connection with the coherent processing associated with range-Doppler mapping. It should be available by spring 1966. Software for the Millstone computer associated with this device will be prepared in a similar time schedule.

(4) Calibration methods for Millstone which use the Lincoln Calibration Sphere (LCS-1) have been worked out and already used in L-band measurements of the lunar cross section to ≈ 0.5 db.* Equipment for facilitating the maintenance of such calibrations over a longer time span is being designed and procured. It is important that similar methods be employed at all radars used in this work.

(5) Microwave hardware has been developed to provide the Millstone radar with great flexibility as regards polarization transmitted, together with ability to receive simultaneously two orthogonal polarizations. This equipment, provided prior to the start of the present contract, made possible the significant polarization studies reported herein.

While it has already been possible to utilize Haystack (at $\lambda = 3.8$ cm) for CW radar planetary observations, commencement of lunar radar measurements at $\lambda = 3.8$ cm depends upon a reliable, efficient pulsed radar capability, which will be available as indicated below. Some Haystack equipment factors are listed as follows:

(1) Work on the series beam-switch regulator and other preparations should permit lunar total cross-section measurements and angular scattering law determinations to begin in March 1966.

(2) Timing and interfacing equipments are largely specified and parts are in procurement which will permit integration of the Haystack processing computer into the radar system for real-time recording and limited processing functions. Complete integration is expected by March or April 1966. Data gathering for lunar mapping can then begin. There will be a speed advantage in utilizing the special equipment at Millstone in conjunction with the Haystack system.

(3) Software developments are also under way including:

   (a) Those required to point the antenna at given places on the moon's surface and to provide the requisite Doppler correction.

   (b) Those required for coherent processing at both radars.

   (c) Those required for conversion from range-Doppler to selenographic coordinates for mapping.

(4) Installation of parts is planned for February and March to permit radar polarization experiments at 3.8 cm, similar in nature to those already carried out at 23 cm.

(5) After many setbacks, 100 kw of RF power can now reliably be generated at X-band in the Haystack radar system.

* Typical measurement accuracies are ±2 or 3 db.

(6) It has been planned to provide for Haystack a slaved boresight optical system, with TV and recording cameras as instrumentation. This system is intended to serve as a check on the Haystack pointing system and to provide data on weather phenomena that could affect the accuracy of measurements at these frequencies. Considerable preliminary work has been accomplished. The ultimate usefulness of this system in the measurement program is being carefully evaluated prior to making major procurements.

The equipment factors discussed in (2) and (3) are designed to enhance the speed of producing a lunar map having the planned few-kilometer resolution. The processing task is large and the final processing speed is yet to be measured. However, there seems little doubt that certain areas of primary importance will have been mapped at Haystack and the results made available in advance of the 1 April 1967 contract completion date. This situation will be re-evaluated as the processing effort proceeds, since some of the processing methods are actually quite new in their details.

The 28-foot millimeter wave facility at Lincoln Laboratory is undergoing considerable refurbishing in preparation for the lunar studies (Fig. 35). The most important single item, however, is the effort to provide substantially more transmitted power than the 12 watts achieved in the measurements of Lynn, et al. (1963). The 8.6-mm results of these workers must be considered preliminary because of the very low signal-to-noise ratios at which they were constrained to work.

After consultation with possible sources, tube procurements have been initiated. A completely new transmitter is being developed to have a 500- to 1000-watt output at 35,000 MHz. Plumbing, feeds, and other components can realistically be tested when the transmitter is available.

D. TIME SCHEDULES

Table VI shows graphically our present best estimates concerning the beginning and end of the periods of most intense activity in connection with the major experiments diagrammed in Figures 34 and 35.

As the schedule indicates, much of the work centered at Millstone is well along. It is likely that results will be at least partially available by the next reporting period.

Planned radiometric work at Haystack has been started. It should be completed on schedule.

Lunar radar work can begin at Haystack as soon as the system can be operated as a pulsed radar. This should take place in early March. Polarization work must await completion of appropriate microwave system features. Certain important items are now in procurement.

In mapping work at Haystack, system stability is vitally important. Certain elements of the frequency control system and its digital controls are critical to this and are presently in procurement. No problem is anticipated in starting this work on schedule. It is expected that software developments and the special processing equipment being obtained to facilitate detailed mapping will permit completion of much of the data reduction in real time.

Completion of the 8.6-mm work is scheduled toward the end of the contractual period because the development of the high power system requires that tube development be completed and that the characteristics of the tube be more clearly defined before transmitter construction can be

TABLE VI

TIME SCHEDULE, PROPOSED MOON EXPERIMENTS

Experiment	CY66 1	CY66 2	CY66 3	CY66 4	CY67 1	CY67 2
23 cm						
2. Polarization Studies	→	→				
3. Cross Section, 4. P(φ), 5. D(φ)	→	→				
6. Polarization Mapping	→	→				
3.8 cm						
1. Radiometric	→	→	→			
3. Cross Section, 4. P(φ), 5. D(φ)		→	→	→		
2. Polarization Studies		→	→	→	→	
7. Detailed Mapping		→	→	→	→	
0.86 cm	Not planned at present. May prove desirable.					
1. Radiometric			→			
3. Cross Section, 4. P(φ), 5. D(φ), 2. Polarization Studies					→	→
Reports to NASA						
Quarterly Progress Report	☒	☒	☒	☒	☒	
Technical Reports, Article Preprints	As prepared					
Final Report						☒

Note: Experiments are numbered to be consistent with Figs. 34 and 35.

started. Measurements of cross section at 8.6 mm should be possible by mid-1966 with a 50-watt system and a lower-temperature front end than used by Lynn. The values obtained will, of course, be refined beginning about 1 January 1967 when the full-power radar should become available.

E. RESPONSIBILITIES

The outline below lists the personnel responsibilities relative to various portions of the Lunar Studies program at Lincoln Laboratory. Except as noted, all personnel are staff members of the Millstone Hill Field Station* of the Radio Physics Division of Lincoln Laboratory.

Principal investigator	P. B. Sebring (Group Leader, in charge of Field Station)
Scientific coordination, overall	Dr. J. V. Evans
Determination of cross section, angular scattering laws, etc.	Dr. J. V. Evans
Polarization studies	Dr. T. Hágfors
Detailed 3.8-cm mapping	Dr. G. H. Pettengill
Radiometric studies	Dr. T. Hagfors; Dr. M. L. Meeks
8-mm radar experiments	Dr. J. J. G. McCue (Radar Division)

ACKNOWLEDGMENTS

The work of most of the technical personnel of Group 31, Surveillance Techniques, which operates the facilities of the Field Station, in preparing and conducting the work reported to date is gratefully acknowledged, as is the work of members of Group 46, Microwave Components, in cooperating with Dr. McCue on the 8.6-mm radar.

The use of the facilities of the Lincoln Laboratory Millstone-Haystack complex, provided by the U.S. Air Force, is also gratefully acknowledged.

* Includes: Millstone L-band tracking radar, UHF ionospheric radar, and the Haystack research facility.

REFERENCES

Beckmann, P., "Radar Backscatter from the Surface of the Moon," J. Geophys. Research 70, 2345-2350 (1965).

Blevis, B.C., "Ionospheric Studies of the Lunar Radar Technique," Nature 180, 138-139 (1957).

_____, and Chapman, J.H., "Characteristics of 488 Megacycles Per Second Radio Signals Reflected from the Moon," J. Research Natl. Bur. Standards 64D, 331-334 (1960).

Bowhill, S.A., "Ionospheric Irregularities Causing Random Fading of Very Low Frequencies," J. Atmos. Terrest Phys. 11, 91-101 (1957).

Bramely, E.N., "A Note on the Theory of Moon Echoes," Proc. Phys. Soc. (London) 80, 1128-1132 (1962).

Brown, W.E., "A Lunar and Planetary Echo Theory," J. Geophys. Research 65, 3087-3095 (1960).

Browne, I.C., et al., "Radio Echoes from the Moon," Proc. Phys. Soc. (London) B69, 901-920 (1956).

Brunschwig, M., et al., "Estimation of the Physical Constants of the Lunar Surface," Report 3544-1-F, University of Michigan, Ann Arbor, Michigan (1960).

Daniels, F.B., "A Theory of Radar Reflection from the Moon and Planets," J. Geophys. Research 66, 1781-1788 (1961).

_____, "Author's Comments on the Preceding Discussion," J. Geophys. Research 67, 895 (1962).

_____, "Radar Determination of the Root Mean Square Slope of the Lunar Surface," J. Geophys. Research 68, 449-453 (1963a).

_____, "Radar Determination of Lunar Slopes: Correction for the Diffuse Component," J. Geophys. Research 68, 2864-2865 (1963b).

Davis, J.R., and Rohlfs, D.C., "Lunar Radio-Reflection Properties at Decameter Wavelengths," J. Geophys. Research 69, 3257-3262 (1964).

DeWitt, J.M., Jr., and Stodola, E.K., "Detection of Radio Signals Reflected from the Moon," Proc. IRE 37, 229-242, (1949).

Dollfus, A., "The Polarization of Moonlight," in Physics and Astronomy of the Moon, Z. Kopal, Ed. (Academic Press, London, 1962), Ch. 5.

Edison, A.R., Moore, R.K., and Warner, B.D., "Radar Return at Near-Vertical Incidence - Summary Report," Technical Report EE-24, University of New Mexico, Albuquerque, New Mexico (1959).

Evans, J.V., "The Scattering of Radiowaves by the Moon," Proc. Phys. Soc. (London) B70, 1105-1112 (1957).

_____, "Radio Echo Studies of the Moon," in Physics and Astronomy of the Moon, Z. Kopal, Ed. (Academic Press, London, 1962a), Ch. 12.

_____, "Radio-Echo Observations of the Moon at 3.6-cm Wavelength," Technical Report 256, Lincoln Laboratory, M.I.T. (1962b), DDC 274669.

_____, "Radio-Echo Observations of the Moon at 68-cm Wavelength," Technical Report 272, Lincoln Laboratory, M.I.T. (1962c), DDC 291102.

_____, Evans, S., and Thomson, J.H., "The Rapid Fading of Moon Echoes at 100 Mc/s," in Paris Symposium on Radio Astronomy, R.N. Bracewell, Ed. (Stanford University Press, Stanford, Calif. 1959), p. 8.

_____, and Hagfors, T., "On the Interpretation of Radar Reflections from the Moon," Icarus 3, 151-160 (1964).

_____, and Ingalls, R.P., "Radio-Echo Studies of the Moon at 7.84-Meter Wavelength," Technical Report 288, Lincoln Laboratory, M.I.T. (1962), DDC 294008.

Evans, J.V., and Pettengill, G.H., "The Radar Cross-Section of the Moon," J. Geophys. Research 68, 5098-5099 (1963a).

_____, "The Scattering Properties of the Lunar Surface at Radio Wavelengths," in The Moon, Meteorites and Comets – The Solar System, Vol. 4, G.P. Kuiper and B.M. Middlehurst, Eds. (University of Chicago Press, Chicago, 1963b), Ch. 5.

_____, "The Scattering Behavior of the Moon at Wavelengths of 3.6, 68 and 784 Centimeters," J. Geophys. Research 68, 423-447 (1963c).

Fricker, S.J., et al., "Characteristics of Moon Reflected UHF Signals," Technical Report 187, Lincoln Laboratory, M.I.T. (1958), DDC 204519.

_____, "Computation and Measurement of the Fading Rate of Moon-Reflected UHF Signals," J. Research Natl. Bur. Standards 64D, 455-465 (1960).

Fung, A.K., and Moore, R.K., "Effects of Structure Size on Moon and Earth Radar Returns at Various Angles," J. Geophys. Research 69, 1075-1081 (1964).

Gold, T., "Processes on the Lunar Surface," in The Moon, Z. Kopal and Z. K. Mikhailov, Eds. (Academic Press, London 1962), p. 433.

_____, private communication.

Grant, C.R., and Yaplee, B.S., "Backscattering from Water and Land at Centimeter and Millimeter Wavelengths," Proc. IRE 45, 976-982 (1957).

Grieg, D.D., Metzger, S., and Waer, R., "Considerations of Moon-Relay Communication," Proc. IRE 36, 652-663 (1948).

Hagfors, T., "Some Properties of Radio Waves Reflected from the Moon and Their Relation to the Lunar Surface," J. Geophys. Research 66, 777-785 (1961).

_____, "Backscattering from an Undulating Surface with Applications to Radar Returns from the Moon," J. Geophys. Research 69, 3779-3784 (1964).

_____, "The Relationship of the Geometric Optics and the Autocorrelation Approaches to the Analysis of Lunar and Planetary Radar Echoes," J. Geophys. Research 71, 379-383 (1966).

_____, Brockelman, R.A., Danforth, H.H., Hanson, L.B., Hyde, G.M., "Tenuous Surface Layer on the Moon: Evidence Derived from Radar Observations," Science 150, 1153-1156 (26 November 1965).

Hapke, B.W., "A Theoretical Photometric Function for the Lunar Surface," J. Geophys. Research 68, 4571-4586 (1963).

_____, and Van Horn, H., "Photometric Studies of Complex Surfaces with Applications to the Moon," J. Geophys. Research 68, 4545-4570 (1963).

Hargreaves, J.K., "Radio Observations of the Lunar Surface," Proc. Phys. Soc. (London) B73, 536-537 (1959).

Hayre, H.S., and Moore, R.K., "Theoretical Scattering Coefficient for Near Vertical Incidence from Contour Maps," J. Research Natl. Bur. Standards 65D, 427-432 (1961).

Heacock, R.L., et al., "Ranger VII Experimenters' Analyses and Interpretations, Parts I and II," JPL-TR-32-700, Jet Propulsion Laboratory, C.I.T. (1965).

Heiles, C.E., and Drake, F.D., "The Polarization and Intensity of Thermal Radiation from a Planetary Surface," Icarus 2, 281-292 (1963).

Hey, J.S., and Hughes, V.A., "Radar Observations of the Moon at 10-cm Wavelength," in Paris Symposium on Radio Astronomy, R.N. Bracewell, Ed. (Stanford University Press, Stanford, Calif. 1959), p. 13.

Hughes, V.A., "Roughness of the Moon as a Radar Reflector," Nature 186, 873-874 (1960).

_____, "Radio Wave Scattering from the Lunar Surface," Proc. Phys. Soc. (London) 78, 988-997 (1961).

_____, "Diffraction Theory Applied to Radio Wave Scattering from the Lunar Surface," Proc. Phys. Soc. (London) 80, 1117-1127 (1962a).

References

Hughes, V.A., "Discussion of Paper by Daniels 'A Theory of Radar Reflections from the Moon and Planets'," J. Geophys. Research 67, 892-894 (1962b).

Kerr, F.J., and Shain, C.A., "Moon Echoes and Transmission Through the Ionosphere," Proc. IRE 39, 230-242 (1951).

Krotikov, V.D., and Troitsky, V.S., "The Emissivity of the Moon at Centimeter Wavelengths," Astron. Zh. 39, 1089-1093 (1962).

Kuiper, G.P., "Interpretation of Ranger VII Records," JPL-TR-32-700, Jet Propulsion Laboratory, C.I.T. (1965), pp. 9-73.

Leadabrand, R.L., et al., "Evidence That the Moon is a Rough Scatterer at Radio Frequencies," J. Geophys. Research 65, 3071-3078 (1960).

Lynn, V.L., Sohigian, M.D., and Crocker, E.A., "Radar Observations of the Moon at 8.6-mm Wavelength," Technical Report 331, Lincoln Laboratory, M.I.T. (1963), DDC 426207. See also, J. Geophys. Research 69, 781-783 (1964).

Markov, A.V., "Brightness Distribution over the Lunar Disk at Full Moon," Astron. Zh. 25, 172-179 (1948).

Mehuron, W.O., "High Resolution Lunar Measurements," presented to the Spring URSI Meeting, Washington, D.C. (1963).

Moore, R.K., and Williams, C.S., Jr., "Radar Terrain Return at Near-Vertical Incidence," Proc. IRE 45, 228-238 (1957).

Muhleman, D.O., "Radar Scattering from Venus and the Moon," Astron. J. 69, 34-41 (1964).

Murray, W.A.S., and Hargreaves, J.K., "Lunar Radar Echoes and the Faraday Effect in the Ionosphere," Nature 173, 944-945 (1954).

Norton, K.A., and Omberg, A.C., "The Maximum Range of a Radar Set," Proc. IRE 35, 4-24 (1947).

O'Keefe, J.A., and Anderson, J.P., "The Earth's Equatorial Radius and the Distance of the Moon," Astron. J. 57, 108-121 (1952).

_____, "Errata," Astron. J. 63, 42, (1958).

Pettengill, G.H., "Measurements of Lunar Reflectivity Using the Millstone Radar," Proc. IRE 48, 933-934 (1960).

_____, private communication.

_____, and Henry, J.C., "Radio Measurements of the Lunar Surface," in The Moon, Z. Kopal and Z.K. Mikhailov, Eds. (Academic Press, London, 1962a), p. 519.

_____, "Enhancement of Radar Reflectivity Associated with the Lunar Crater Tycho," J. Geophys. Research 67, 4881-4885 (1962b).

Rea, R.D., Hetherington, N., and Mifflin, R., "The Analysis of Radar Echoes from the Moon," J. Geophys. Research 69, 5217-5223 (1964).

Rice, S.O., "Mathematical Analysis of Random Noise," Bell System Tech. J. 23, 282-332 (1944).

_____, "Mathematical Analysis of Random Noise," Bell System Tech. J. 24, 46-156 (1945).

Saari, J.M., and Shorthill, R.W., "Thermal Anomalies on the Totally Eclipsed Moon of December 19, 1964," Nature 205, 964-965 (1965).

Safran, H., "Back-Scattering Properties of Moon and Earth at X-Band," AIAA J. 2, 100-101 (1964).

Salomonovich, A.E., and Losovsky, B.Y., "Radio Brightness Distribution of the Lunar Disk at 0.8 cm," Astron. Zh. 39, 1074-1082 (1962).

Schoenberg, E., "Theoretische Photometrie," in Handbuch der Astrophysik, Part 2, Vol. I (Springer, Berlin, 1929), Ch. I.

Senior, T.B.A., and Siegel, K.M., "Radar Reflection Characteristics of the Moon," in Paris Symposium on Radio Astronomy, R.N. Bracewell, Ed. (Stanford University Press, Stanford, Calif. 1959), p. 29.

Senior, T.B.A., and Siegel, K.M., "A Theory of Radar Scattering by the Moon," J. Research Natl. Bur. Standards 64D, 217-228 (1960).

Shorthill, R.W., "Measurements of Lunar Temperature Variations During an Eclipse and Throughout a Lunation," Boeing Report D.1. 82-0196, Boeing Scientific Research Laboratories, Seattle, Wash. (1962).

Soboleva, N.S., "Measurement of the Polarization of Lunar Radio Emission on a Wavelength of 3.2 cm," Astron. Zh. 39, 1124-1126 (1962).

Thomas, A.B., "Certain Physical Constants and Their Relation to the Doppler Shift in Radio Echoes from the Moon," Austral J. Sci. 11, 187-192 (1949).

Thompson, T.W., "Enhanced Radar Scattering of Young and Rayed Craters," Ph.D. Thesis, Cornell University, Ithaca, N.Y. (September 1965).

Trexler, J.H., "Lunar Radio Echoes," Proc. IRE 46, 286-292 (1958).

Troitsky, V.S., "Radio Emission of the Moon, Its Physical State and the Nature of Its Surface," in The Moon, Z. Kopal and Z. Mikhailov, Eds. (Academic Press, London, 1962), p. 475.

Twersky, V., "On Scattering of Waves by Random Distributions, II. Two Space Scatterer Formalism," J. Math. Phys. 3, 724-734 (1962).

Victor, W.K., Stevens, R., and Golomb, S.W., "Radar Exploration of Venus," JPL-TR-32-132, Jet Propulsion Laboratory, C.I.T. (1961).

Von Biel, H.A., "An Experimental Investigation of Lunar and Auroral Scattered Signals – Part I: Lunar Echoes," AFCRL-62-78, Air Force Cambridge Research Laboratories, Lexington, Mass. (1962), DDC 273686.

Winter, D.F., "A Theory of Radar Reflections from a Rough Moon," J. Research Natl. Bur. Standards 66D, 215, 226 (1962).

Yaplee, B.S., et al., "Radar Echoes from the Moon at a Wavelength of 10 cm," Proc. IRE 46, 293-297 (1958).

_____, "A Lunar Radar Study at 10-cm Wavelength," Paris Symposium on Radio Astronomy, R.N. Bracewell, Ed. (Stanford University Press, Stanford, Calif. 1959), p. 19.

_____, et al., "The Mean Distance to the Moon as Determined by Radar," Report 6134, Naval Research Laboratory, Bethesda, Md. (1964).